# Spectral asymmetries in ground-state grating and stimulated emission pumping configurations of two-color resonant four-wave-mixing spectroscopy

A. A. Villaeys*
*Institut de Physique et Chimie des Matériaux de Strasbourg 23, rue du Loess, 67037 Strasbourg Cedex, France*
(Received 16 April 2001; published 10 May 2002)

The recent evolution toward resonant conditions of the two-color resonant four-wave-mixing (TC-RFWM) spectroscopy has been dictated by the high sensitivity required experimentally. While some models have been used in different contexts such as light pressure forces in strong polychromatic fields, magnetically assisted Sisyphus effect, or multiphoton resonances in $\Lambda$ atoms, the existence in molecules of additional processes such as nonradiative transitions and rotational or vibrational dephasings requires the extension of previous models. For this reason, we give here a general description of the internal dynamics for a molecule undergoing two strong grating beams, acting either on two different transitions sharing a common level or on the same transition, and one weak probe beam to reproduce the ground-state grating and stimulated emission pumping configurations of TC-RFWM spectroscopy. By combining high spectral resolution and strong grating beams, we show that the TC-RFWM spectrum is very sensitive to the transition constants, dephasing constants, as well as to the transverse velocity of the molecules in the jet. The last case corresponding to a bichromatic field acting on a single transition is used to explain the origin of the line-shape asymmetry observed experimentally on jet-cooled molecules.

DOI: 10.1103/PhysRevA.65.053822 PACS number(s): 42.65.Hw, 42.65.Ky

## I. INTRODUCTION

While most of the nonlinear optical spectroscopic techniques are based on nonresonant excitations to preserve the characteristics of the intrinsic dynamics of the materials under investigation [1,2], more recently there was a need to improve the sensitivity of the emitted signals. This is particularly true for the detection of traces and transient species in low-density environments, such as free-jet expansions. Among the resonant methods, resonant four-wave mixing (RFWM) and degenerate four-wave mixing (DFWM) pertain to a broad class of nonlinear optical processes that have been extensively used in spectroscopy to study the spectral characteristics of transient and stable molecules [3–5]. Besides, the resonant character of these methods offers distinct advantages over linear techniques to study the structure and dynamics of molecular systems in the gas phase. We note that it is a coherent, background-free technique with favorable signal-to-noise ratios. In addition, because the signal is based only on absorption and not on a particular decay mode for detection, any excited state may be probed regardless of its decay mode such as ionization, dissociation, or fluorescence. For this reason, these techniques are very attractive in state-selective spectroscopy [6,7].

Few years ago, taking advantage of models previously developed in atomic physics [8–14], particular schemes like V and $\Lambda$ models have been the starting point of new spectroscopic techniques. The case of the termed two-color resonant four-wave mixing (TC-RFWM) is of special interest and has been used to perform a number of experiments [15,16]. This is particularly the case in the determination of the background-free stimulated emission pumping spectrum of stable NO [17] and the transient species of $C_3$ and HCO [18]. Due to the weak-field regime adopted in this last experiment, the theoretical description introduced to test their experimental results is based on a diagrammatic perturbation theory and spherical tensor analysis. By extending a previous treatment on DFWM [19], the authors have established an expression for the signal intensity for TC-RFWM that accounts for polarization and relaxation effects. Also, TC-RFWM spectroscopy has potential applications to our understanding of the dynamics of excited states that decay rapidly by intramolecular nonradiative processes. In particular, this technique has been used to study predissociating and autoionizing states in nitric oxide [20,21]. The superiority of TC-RFWM in detecting strongly predissociative states of CH has been clearly demonstrated by characterizing the bands (0-0) and (1-0) of the $B\ ^2\Sigma^- - X\ ^2\Pi$ transition [22] and the (1-1) band of the $C\ ^2\Sigma^+ - X\ ^2\Pi$ transition of CH [23], using a ground-state double-resonance scheme in which two transitions share the common lower level $X\ ^2\Pi$. With the same theoretical approach previously mentioned, a signal line profile, observed by probing an isolated quasibound state described by a configuration interaction, has been developed recently to evaluate the contributions to third-order susceptibility of TC-RFWM [24]. Due to the weak intensities for the excitation laser beams, most of these experiments have been done in the nonsaturated limit, and have been described in terms of perturbational expansion. This is also the case in the work done by Williams, Zare, and Rahn [5] to derive expressions via time-independent diagrammatic perturbation theory that account for DFWM polarization, collisional, and velocity effects for levels with definite angular momentum. This treatment has been extended to the analysis of the dependence on beam polarizations and rotational branch combinations of the TC-RFWM spectra [25,26].

More recently, DFWM and TC-RFWM techniques have been extended to bridge between the weak- and strong-field

*FAX: 33 3 88 10 72 50.
Email address: albert.villaeys@ipcms.u-strasbg.fr

 

regimes. These treatments are mostly based on the Abrams-Lind model of DFWM on a nondegenerate homogeneously broadened two-level system [27–29]. One interesting peculiarity of this model is that the DFWM signal is insensitive to collisions when the intensity of the pump field is increased enough, so that the population difference oscillates at a Rabi frequency greater than the relaxation and dephasing rates. However, this model is restricted to the case of monochromatic laser beams of the same polarization state and phase conjugation geometry. This model has been extended to broad-bandwidth lasers whose time dependence can be solved numerically [30]. Also, a more general description was given for degenerate four-wave mixing with broadband lasers [31,32], which exhibits qualitative agreement with experiments [30]. The first experimental observation of a dip by TC-RFWM was obtained by using two-color laser-induced grating spectroscopy to obtain the $S_1$-$S_0$ excitation spectra of jet-cooled azulene [33]. Later, a saturation dip has been observed in DFWM and TC-RFWM spectra of jet-cooled CH generated from laser photolysis of $CHBr_3$ [34]. In this experiment, the common frequency of two nearly parallel grating beams is tuned around the frequency of the *B*-*X* (0-0) vibronic band while the probe beam frequency is held fixed at the frequency of the *A*-*X* (0-0) transition. For increasing intensities of the grating beams, the spectral line of the *B*-*X* (0-0) vibronic band becomes broadened and then develops a dip resulting in a splitting of the line. In addition, it has been clearly established that the threshold for saturation dip of various lines in this band correlates with their greatest absorption cross section. Also, the threshold is very sensitive to the various polarization schemes that can be used in this experiment with the *YYYY* scheme showing the smallest saturation threshold. Because the small transverse velocity component in the jet beam along the direction of the input laser beams cannot explain the line splitting, the results have been interpreted by using the theory of DFWM given by Meacher and co-workers with broadband lasers [30–32]. However, with respect to these recent experimental results obtained by TC-RFWM and DFWM experiments on jet-cooled CH [34], if this theory simulates correctly the DFWM lines profiles as well as the depth of the saturation dip for increasing intensity of the laser beam, it fails to describe the asymmetry of the TC-RFWM spectra, as well as to account for the polarization effects.

In the present work, we give a general description of the dynamics taking place in a V-or Λ-like model undergoing transitions between its excited states, as well as relaxations and pure dephasings. The first case under investigation in the present work concerns a situation where two strong beams act on two different transitions sharing a common level and a weak beam probing one transition, a method that enables to develop a high selectivity. The second case corresponds to a bichromatic beam acting on one transition while the second transition is tested by the probe beam. Peculiar features observed on TC-RFWM spectra are recovered.

## II. DYNAMICAL EVOLUTION INDUCED BY THE STRONG GRATING BEAMS ACTING ON TWO DIFFERENT TRANSITIONS

The traditional interpretation of a TC-RFWM spectroscopy corresponds to the laser-induced grating picture. In such an experiment, shown in Fig. 1, two nearly copropagating grating beams nearly resonant with either the same or two different transitions overlap at a small angle on the sample creating a diffraction grating resulting from the subsequent spatial modulation. Then a third beam, the probe beam, with a weaker intensity is scattered by the diffraction grating and creates a four-wave-mixing signal. The strong stationary grating fields $\mathbf{E}_p(\mathbf{r},t)$ and $\mathbf{E}_t(\mathbf{r},t)$ are described by

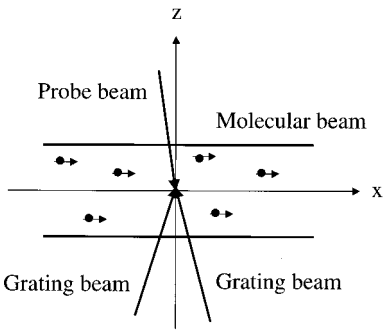


FIG. 1. Geometry required in a TC-RFWM experiment performed on a molecular jet beam.

$$\mathbf{E}_u(\mathbf{r},t)=\mathbf{E}_u(\Omega_u)\exp(-i\Omega_u t+i\mathbf{k}_u\cdot\mathbf{r})+\text{c.c.},\quad u=p,t \tag{2.1}$$

with frequency $\Omega_u$ and wave vector $\mathbf{k}_u$. The quantity $\mathbf{E}_u(\Omega_u)$ accounts for the amplitude and polarization of the field. Most of the experiments in TC-RFWM require V- or Λ-type models [9,12–14] and correspond to the termed ground-state grating (GSG) and stimulated emission pumping (SEP) configurations, where two strong light beams are applied on two different transitions sharing a common level, as represented in Fig. 2. The dynamical evolution induced by the strong grating beams can be treated on the same footing for both models, since their corresponding dynamical evolutions differ by the initial conditions only. The basic model will be described by a three-level system. For the sake of

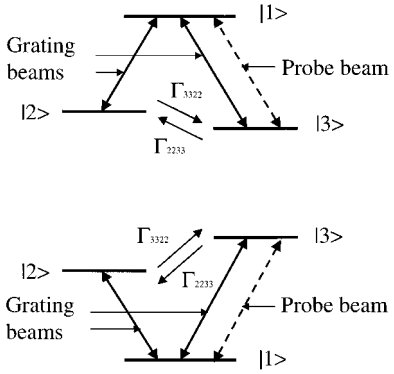


FIG. 2. Energetic level structures associated with the V model and Λ model for the SEP spectroscopy (bottom) and GSG spectroscopy, respectively. Here, the grating beams act on different transitions. The transitions excited by the grating beams and the probe beams are shown in the figure. The system can support nonradiative processes.

simplicity, we will refer to the state $|1\rangle$ as the ground state and states $|2\rangle$ and $|3\rangle$ as the excited states, but this is only a matter of convenience. In contradiction to models previously developed, the model must be able to account for different relaxation and dephasing constants, which is not the case in atomic physics [9–12], and must support transition processes. The general evolution of the populations and coherences are given by

$$\begin{aligned}
\frac{d\rho_{11}}{dt} &= \frac{i}{\hbar}\boldsymbol{\mu}_{12}\cdot\mathbf{E}_p(\mathbf{r},t)\rho_{21} - \frac{i}{\hbar}\rho_{12}\boldsymbol{\mu}_{21}\cdot\mathbf{E}_p(\mathbf{r},t) \\
&\quad + \frac{i}{\hbar}\boldsymbol{\mu}_{13}\cdot\mathbf{E}_t(\mathbf{r},t)\rho_{31} - \frac{i}{\hbar}\rho_{13}\boldsymbol{\mu}_{31}\cdot\mathbf{E}_t(\mathbf{r},t) - \Gamma_{1111}\rho_{11} \\
&\quad - \Gamma_{1122}\rho_{22} - \Gamma_{1133}\rho_{33}, \\
\frac{d\rho_{22}}{dt} &= \frac{i}{\hbar}\boldsymbol{\mu}_{21}\cdot\mathbf{E}_p(\mathbf{r},t)\rho_{12} - \frac{i}{\hbar}\rho_{21}\boldsymbol{\mu}_{12}\cdot\mathbf{E}_p(\mathbf{r},t) - \Gamma_{2211}\rho_{11} \\
&\quad - \Gamma_{2222}\rho_{22} - \Gamma_{2233}\rho_{33}, \\
\frac{d\rho_{33}}{dt} &= \frac{i}{\hbar}\boldsymbol{\mu}_{31}\cdot\mathbf{E}_t(\mathbf{r},t)\rho_{13} - \frac{i}{\hbar}\rho_{31}\boldsymbol{\mu}_{13}\cdot\mathbf{E}_t(\mathbf{r},t) - \Gamma_{3311}\rho_{11} \\
&\quad - \Gamma_{3322}\rho_{22} - \Gamma_{3333}\rho_{33}, \\
\frac{d\rho_{12}}{dt} &= [i\omega_{21} - \Gamma_{1212}]\rho_{12} + \frac{i}{\hbar}\boldsymbol{\mu}_{12}\cdot\mathbf{E}_p(\mathbf{r},t)[\rho_{22} - \rho_{11}] \\
&\quad + \frac{i}{\hbar}\boldsymbol{\mu}_{13}\cdot\mathbf{E}_t(\mathbf{r},t)\rho_{32}, \\
\frac{d\rho_{13}}{dt} &= [i\omega_{31} - \Gamma_{1313}]\rho_{13} + \frac{i}{\hbar}\boldsymbol{\mu}_{13}\cdot\mathbf{E}_t(\mathbf{r},t)[\rho_{33} - \rho_{11}] \\
&\quad + \frac{i}{\hbar}\boldsymbol{\mu}_{12}\cdot\mathbf{E}_p(\mathbf{r},t)\rho_{23}, \\
\frac{d\rho_{23}}{dt} &= [i\omega_{32} - \Gamma_{2323}]\rho_{23} + \frac{i}{\hbar}\boldsymbol{\mu}_{21}\cdot\mathbf{E}_p(\mathbf{r},t)\rho_{13} \\
&\quad - \frac{i}{\hbar}\rho_{21}\boldsymbol{\mu}_{13}\cdot\mathbf{E}_t(\mathbf{r},t),
\end{aligned} \tag{2.2}$$

where $d/dt \equiv \partial/\partial t + \mathbf{v}(\partial/\partial\mathbf{r})$. Of course, the rates $\Gamma_{iijj}$ are algebric quantities according to the closure relation $\Gamma_{iiii} = -\Sigma_{j\neq i}\Gamma_{iijj}$ ensuring the incoherent balance of populations between the levels of the systems. In the following, we introduce the notation $\omega_{ij} = \omega_i - \omega_j$ and assume that the near-resonant conditions

$$\begin{aligned}
&|\Omega_p - \omega_{21}| \ll \omega_{21}, \omega_{31}, |\omega_{21} - \omega_{31}|, \\
&|\Omega_t - \omega_{31}| \ll \omega_{21}, \omega_{31}, |\omega_{21} - \omega_{31}|
\end{aligned} \tag{2.3}$$

are satisfied. Also, we have the usual relation $\Gamma_{ijij} = 1/2[\Gamma_{iiii} + \Gamma_{jjjj}] + \Gamma_{ij}^{(d)}$ between the dephasing constants, total decay rates, and pure dephasing constants. Notice that the transition constants are related by the detailed balance equation $\Gamma_{3322} = \Gamma_{2233} e^{-\hbar\omega_{32}/kT}$. For near-resonant fields, the rotating-wave approximation can be used and the corresponding radiation-matter interaction takes the form

$$\begin{aligned}
V_{p,mn}^{\mathrm{RWA}}(t) &= -\boldsymbol{\mu}_{mn}\cdot\mathbf{E}_p(\varepsilon_{mn}\Omega_p)\exp[-i\varepsilon_{mn}(\Omega_p t - \mathbf{k}_p\cdot\mathbf{r})], \\
V_{t,mn}^{\mathrm{RWA}}(t) &= -\boldsymbol{\mu}_{mn}\cdot\mathbf{E}_t(\varepsilon_{mn}\Omega_t)\exp[-i\varepsilon_{mn}(\Omega_t t - \mathbf{k}_t\cdot\mathbf{r})],
\end{aligned} \tag{2.4}$$

where the symbol $\varepsilon_{mn}$ is equal to $+1$ or $-1$ depending on whether the energy gap between the states $|m\rangle$ and $|n\rangle$, corresponding to $(\omega_m - \omega_n)$, is positive or negative, respectively. Also, we have the relation between the field amplitudes, $\mathbf{E}_u(-\Omega_u) = \mathbf{E}_u^*(\Omega_u)$. In the following, we introduce the new variables

$$\begin{aligned}
\sigma_{12} &= \rho_{12}\exp(-i\Omega_p t + i\mathbf{k}_p\cdot\mathbf{r}), \\
\sigma_{13} &= \rho_{13}\exp(-i\Omega_t t + i\mathbf{k}_t\cdot\mathbf{r}), \\
\sigma_{23} &= \rho_{23}\exp[i(\Omega_p - \Omega_t)t - i(\mathbf{k}_p - \mathbf{k}_t)\cdot\mathbf{r}], \\
\sigma_{ii} &= \rho_{ii} \quad \forall \quad i = 1,\ 2,\ 3,
\end{aligned} \tag{2.5}$$

as well as the Rabi frequencies

$$\hbar\Omega_R(12,p) = \boldsymbol{\mu}_{12}\cdot\mathbf{E}_p^*(\Omega_p), \quad \hbar\Omega_R(13,t) = \boldsymbol{\mu}_{13}\cdot\mathbf{E}_t^*(\Omega_t), \tag{2.6}$$

which are assumed real. Notice that because of the beam geometry very often adopted in these experiments, with grating beams almost perpendicular to the molecular-beam axis, we have $d/dt \equiv \partial/\partial t + v_z(\partial/\partial z)$. Also, the ground state is stable, $\Gamma_{1111} = 0$, and transitions from the ground state to the excited states are not allowed spontaneously by the surrounding medium, so that $\Gamma_{2211} = \Gamma_{3311} = 0$. This implies that we emphasize more on the GSG configuration, but the SEP configuration can be obtained along the same lines with $\Gamma_{2222} = 0$. Finally, in terms of the population differences

$$\begin{aligned}
\eta_{21} &= \sigma_{22} - \sigma_{11}, \\
\eta_{31} &= \sigma_{33} - \sigma_{11},
\end{aligned} \tag{2.7}$$

the probability conservation $\Sigma_{i=1}^{3}\ \sigma_{ii} = 1$ gives

$$\begin{aligned}
\sigma_{22} &= \tfrac{2}{3}\eta_{21} - \tfrac{1}{3}\eta_{31} + \tfrac{1}{3}, \\
\sigma_{33} &= -\tfrac{1}{3}\eta_{21} + \tfrac{2}{3}\eta_{31} + \tfrac{1}{3}.
\end{aligned} \tag{2.8}$$

Then, the set of Eqs. (2.2) takes the form

$$\begin{aligned}
\frac{\partial\eta_{21}}{\partial t} &= -2i\Omega_R(12,p)\sigma_{21} + 2i\Omega_R(21,p)\sigma_{12} - i\Omega_R(13,t)\sigma_{31} \\
&\quad + i\Omega_R(31,t)\sigma_{13} - (\Gamma_{2222} - \Gamma_{1122})[\tfrac{2}{3}\eta_{21} - \tfrac{1}{3}\eta_{31} + \tfrac{1}{3}] \\
&\quad - (\Gamma_{2233} - \Gamma_{1133})[-\tfrac{1}{3}\eta_{21} + \tfrac{2}{3}\eta_{31} + \tfrac{1}{3}],
\end{aligned}$$

$$\frac{\partial \eta_{31}}{\partial t} = 2i\Omega_R(31,t)\sigma_{13} - 2i\Omega_R(13,t)\sigma_{31} + i\Omega_R(21,p)\sigma_{12} - i\Omega_R(12,p)\sigma_{21} - (\Gamma_{3322}-\Gamma_{1122})[\tfrac{2}{3}\eta_{21} - \tfrac{1}{3}\eta_{31} + \tfrac{1}{3}] - (\Gamma_{3333}-\Gamma_{1133})[-\tfrac{1}{3}\eta_{21} + \tfrac{2}{3}\eta_{31} + \tfrac{1}{3}],$$

$$\frac{\partial \sigma_{12}}{\partial t} = [i(\omega_{21} - \Omega_p + k_{pz}v_z) - \Gamma_{1212}]\sigma_{12} + i\Omega_R(12,p)\eta_{21} + i\Omega_R(13,t)\sigma_{32},$$

$$\frac{\partial \sigma_{13}}{\partial t} = [i(\omega_{31} - \Omega_t + k_{tz}v_z) - \Gamma_{1313}]\sigma_{13} + i\Omega_R(13,t)\eta_{31} + i\Omega_R(12,p)\sigma_{23},$$

$$\frac{\partial \sigma_{23}}{\partial t} = [i(\omega_{32} + \Omega_p - \Omega_t - k_{pz} + k_{tz}) - \Gamma_{2323}]\sigma_{23} + i\Omega_R(21,p)\sigma_{13} - i\Omega_R(13,t)\sigma_{21}, \tag{2.9}$$

where, as usual, the $z$ dependence of the various $\sigma_{ij}$ has been neglected. We first define the real and imaginary parts of the coherences by the expression

$$\sigma_{mn}(t) = \sigma_{\mathrm{Re}\,mn}(t) + i\sigma_{\mathrm{Im}\,mn}(t). \tag{2.10}$$

To solve the set of Eqs. (2.9), we introduce for each real quantity $\eta_{21}(t)$, $\eta_{31}(t)$, $\sigma_{\mathrm{Re}\,12}(t)$, $\sigma_{\mathrm{Im}\,12}(t)$, $\sigma_{\mathrm{Re}\,13}(t)$, $\sigma_{\mathrm{Im}\,13}(t)$, $\sigma_{\mathrm{Re}\,23}(t)$, and $\sigma_{\mathrm{Im}\,23}(t)$, the Fourier series

$$u(t) = \sum_{n=-\infty}^{\infty} u^{(n)}(\omega)e^{in\omega t}. \tag{2.11}$$

They give, in turn, the set of equations

$$(in\omega + \alpha_1)\eta_{21}^{(n)}(\omega) = \alpha_2\eta_{31}^{(n)}(\omega) - \alpha_3\delta_{n,0} - 4\Omega_R(21,p) \times \sigma_{\mathrm{Im}\,12}^{(n)}(\omega) - 2\Omega_R(31,t)\sigma_{\mathrm{Im}\,13}^{(n)}(\omega),$$

$$(in\omega + \beta_1)\eta_{31}^{(n)}(\omega) = \beta_2\eta_{21}^{(n)}(\omega) - \beta_3\delta_{n,0} - 4\Omega_R(31,t) \times \sigma_{\mathrm{Im}\,13}^{(n)}(\omega) - 2\Omega_R(21,p)\sigma_{\mathrm{Im}\,12}^{(n)}(\omega),$$

$$(in\omega + \Gamma_{1212})\sigma_{\mathrm{Re}\,12}^{(n)}(\omega) = -(\omega_{21} - \Omega_p + k_{pz}v_z)\sigma_{\mathrm{Im}\,12}^{(n)}(\omega) + \Omega_R(13,t)\sigma_{\mathrm{Im}\,23}^{(n)}(\omega),$$

$$(in\omega + \Gamma_{1212})\sigma_{\mathrm{Im}\,12}^{(n)}(\omega) = (\omega_{21} - \Omega_p + k_{pz}v_z)\sigma_{\mathrm{Re}\,12}^{(n)}(\omega) + \Omega_R(12,p)\eta_{21}^{(n)}(\omega) + \Omega_R(13,t)\sigma_{\mathrm{Re}\,23}^{(n)}(\omega),$$

$$(in\omega + \Gamma_{1313})\sigma_{\mathrm{Re}\,13}^{(n)}(\omega) = -(\omega_{31} - \Omega_t + k_{tz}v_z)\sigma_{\mathrm{Im}\,13}^{(n)}(\omega) - \Omega_R(12,p)\sigma_{\mathrm{Im}\,23}^{(n)}(\omega),$$

$$(in\omega + \Gamma_{1313})\sigma_{\mathrm{Im}\,13}^{(n)}(\omega) = (\omega_{31} - \Omega_t + k_{tz}v_z)\sigma_{\mathrm{Re}\,13}^{(n)}(\omega) + \Omega_R(13,t)\eta_{31}^{(n)}(\omega) + \Omega_R(12,p)\sigma_{\mathrm{Re}\,23}^{(n)}(\omega),$$

$$(in\omega + \Gamma_{2323})\sigma_{\mathrm{Re}\,23}^{(n)}(\omega) = -(\omega_{32} - \Omega_t + \Omega_p + k_{tz}v_z - k_{pz}v_z)\sigma_{\mathrm{Im}\,23}^{(n)}(\omega) - \Omega_R(21,p)\sigma_{\mathrm{Im}\,13}^{(n)}(\omega) - \Omega_R(13,t)\sigma_{\mathrm{Im}\,12}^{(n)}(\omega),$$

$$(in\omega + \Gamma_{2323})\sigma_{\mathrm{Im}\,23}^{(n)}(\omega) = (\omega_{32} - \Omega_t + \Omega_p + k_{tz}v_z - k_{pz}v_z)\sigma_{\mathrm{Re}\,23}^{(n)}(\omega) + \Omega_R(21,p)\sigma_{\mathrm{Re}\,13}^{(n)}(\omega) - \Omega_R(13,t)\sigma_{\mathrm{Re}\,12}^{(n)}(\omega), \tag{2.12}$$

with $\delta_{ij}$ the Kronecker symbol. We finally get the previous equation in the general form

$$M^{(n)}(\omega)\boldsymbol{\Sigma}^{(n)}(\omega) = \boldsymbol{\Lambda}\delta_{n,0}, \tag{2.13}$$

where $\boldsymbol{\Sigma}^{(l)}(\omega)$ and $\boldsymbol{\Lambda}$ stand for the vectors with components

$$\boldsymbol{\Sigma}^{(l)}(\omega) = \{(\eta_{21}^{(l)}(\omega), \eta_{31}^{(l)}(\omega), \sigma_{\mathrm{Re}\,12}^{(l)}(\omega), \sigma_{\mathrm{Im}\,12}^{(l)}(\omega), \times\sigma_{\mathrm{Re}\,13}^{(l)}(\omega), \sigma_{\mathrm{Im}\,13}^{(l)}(\omega), \sigma_{\mathrm{Re}\,23}^{(l)}(\omega), \sigma_{\mathrm{Im}\,23}^{(l)}(\omega)\},$$

$$\boldsymbol{\Lambda} = \{\alpha_3, \beta_3, 0, 0, 0, 0, 0, 0\}. \tag{2.14}$$

Also, the additional notations

$$3\alpha_1 = 2(\Gamma_{2222}-\Gamma_{1122}) - (\Gamma_{2233}-\Gamma_{1133}),$$

$$3\alpha_2 = (\Gamma_{2222}-\Gamma_{1122}) - 2(\Gamma_{2233}-\Gamma_{1133}),$$

$$3\alpha_3 = (\Gamma_{2222}-\Gamma_{1122}) + (\Gamma_{2233}-\Gamma_{1133}),$$

$$3\beta_1 = -(\Gamma_{3322}-\Gamma_{1122}) + 2(\Gamma_{3333}-\Gamma_{1133}),$$

$$3\beta_2 = -2(\Gamma_{3322}-\Gamma_{1122}) + (\Gamma_{3333}-\Gamma_{1133}),$$

$$3\beta_3 = (\Gamma_{3322}-\Gamma_{1122}) + (\Gamma_{3333}-\Gamma_{1133}), \tag{2.15}$$

have been introduced. The matrix $M^{(n)}(\omega)$ corresponds to

$$M^{(n)}(\omega)=\begin{pmatrix} in\omega-\alpha_1 & \alpha_2 & 0 & -4\Omega_R(21,p) & 0 & -2\Omega_R(31,t) & 0 & 0 \\ \beta_2 & -in\omega-\beta_1 & 0 & -2\Omega_R(21,p) & 0 & -4\Omega_R(31,t) & 0 & 0 \\ 0 & 0 & -in\omega-\Gamma_{1212} & -\omega_{21}+\Omega_p' & 0 & 0 & 0 & \Omega_R(13,t) \\ \Omega_R(12,p) & 0 & \omega_{21}-\Omega_p' & -in\omega-\Gamma_{1212} & 0 & 0 & \Omega_R(13,t) & 0 \\ 0 & 0 & 0 & 0 & -in\omega-\Gamma_{1313} & -\omega_{31}+\Omega_t' & 0 & -\Omega_R(12,p) \\ 0 & \Omega_R(13,t) & 0 & 0 & \omega_{31}-\Omega_t' & -in\omega-\Gamma_{1313} & \Omega_R(12,p) & 0 \\ 0 & 0 & 0 & -\Omega_R(13,t) & 0 & -\Omega_R(21,p) & -in\omega-\Gamma_{2323} & -\omega_{32}+\Omega_t'-\Omega_p' \\ 0 & 0 & -\Omega_R(13,t) & 0 & \Omega_R(21,p) & 0 & \omega_{32}-\Omega_t'+\Omega_p' & -in\omega-\Gamma_{2323} \end{pmatrix} \tag{2.16}$$

if the symbols $\Omega_u'=\Omega_u-k_{uz}v_z$ with $u=p,\ t$ are introduced. The evaluation of the density matrix elements $\rho_{ij}(t)$ requires the solution of Eq. (2.12) for the various values of $n$. We first consider the terms $n=0$. Here, we are left with the inhomogeneous linear system

$$M^{(0)}(\omega)\mathbf{\Sigma}^{(0)}(\omega)=\mathbf{\Lambda}, \tag{2.17}$$

and the solution for the $k$th component $\Sigma_k^{(0)}(\omega)$ takes the form

$$\Sigma_k^{(0)}(\omega)=\det N_{(k)}^{(0)}(\omega)/\det M^{(0)}(\omega), \tag{2.18}$$

where the matrix $N_{(k)}^{(0)}(\omega)$ is defined by

$$N_{(k)ij}^{(0)}(\omega)=M_{ij}^{(0)}(\omega) \quad \forall\ i \quad \text{and} \quad \forall\ j\neq k,$$

$$N_{(k)ij}^{(0)}(\omega)=\Lambda_i \quad \forall\ i \ \text{with}\ j=k. \tag{2.19}$$

We come now to the terms $n\neq 0$. In that case, we are looking for the solutions of an homogeneous linear equation system whose trivial solution is

$$\mathbf{\Sigma}^{(n)}(\omega)=0. \tag{2.20}$$

Notice that this solution corresponds to the steady-state case often encountered in the literature, implying no time dependence for the populations and coherences evolving with the frequencies of the fields. This is the direct consequence of the rotating-wave approximation introduced at the beginning of the calculation. If this assumption is relaxed, we necessarily have a coupling between different values of $n$, whose corresponding contributions are generated recurrently from the term $n=0$ in the form of a continued fraction expansion [8,11,35].

## III. DESCRIPTION OF THE PROBING PROCESS AND THE RESULTING DYNAMICS

The probe beam introduced to test the diffraction grating has a much weaker intensity than the grating beams. It will be described using similar notations previously used for the strong grating beams, and can be expressed as

$$\mathbf{E}_s(\mathbf{r},t)=\mathbf{E}_s(\Omega_s)\exp(-i\Omega_s t+i\mathbf{k}_s\cdot\mathbf{r})+\text{c.c.} \tag{3.1}$$

This beam will be applied on the $|1\rangle\rightarrow|3\rangle$ transition as shown in Fig. 2 and will be treated perturbatively. From the dynamical point of view, the system described as a V model excited by two strong beams $\mathbf{E}_p(\mathbf{r},t)$ and $\mathbf{E}_t(\mathbf{r},t)$, each one being applied on a different transition, is now tested by a weak probe beam $\mathbf{E}_s(\mathbf{r},t)$. Therefore, besides the dynamics induced by the two strong beams, which are accounted for rigorously and have been described in the preceding section, we must introduce the additional weak probe beam perturbatively. First, we describe the dynamical equations for the zero- and first-order contributions to the density matrix $\rho(t)$. They correspond to $\rho^{(0)}(t)$ and $\rho^{(1)}(t)$ and are solutions of

$$\frac{d\rho^{(0)}(t)}{dt}=-\frac{i}{\hbar}[H_0+V^{(0)},\rho^{(0)}]-\Gamma\rho^{(0)},$$

$$\frac{d\rho^{(1)}(t)}{dt}=-\frac{i}{\hbar}[H_0+V^{(0)},\rho^{(1)}]-\frac{i}{\hbar}[V^{(1)},\rho^{(0)}]-\Gamma\rho^{(1)}. \tag{3.2}$$

In the particular case of a V model, the first equation has been solved previously. Then, we are left with the resolution of the second equation giving the first-order contributions. For the various matrix elements $\rho_{ij}^{(1)}(t)$, we get

$$\frac{d\rho_{11}^{(1)}}{dt}=-\frac{i}{\hbar}[V_{12}^{(0)}\rho_{21}^{(1)}-\rho_{12}^{(1)}V_{21}^{(0)}+V_{13}^{(0)}\rho_{31}^{(1)}-\rho_{13}^{(1)}V_{31}^{(0)} + V_{13}^{(1)}\rho_{31}^{(0)}-\rho_{13}^{(0)}V_{31}^{(1)}]-\Gamma_{1122}\rho_{22}^{(1)}-\Gamma_{1133}\rho_{33}^{(1)},$$

$$\frac{d\rho_{22}^{(1)}}{dt}=-\frac{i}{\hbar}\{V_{21}^{(0)}\rho_{12}^{(1)}-\rho_{21}^{(1)}V_{12}^{(0)}\}-\Gamma_{2222}\rho_{22}^{(1)}-\Gamma_{2233}\rho_{33}^{(1)},$$

$$\frac{d\rho_{33}^{(1)}}{dt}=-\frac{i}{\hbar}\{V_{31}^{(0)}\rho_{13}^{(1)}-\rho_{31}^{(1)}V_{13}^{(0)}+V_{31}^{(1)}\rho_{13}^{(0)}-\rho_{31}^{(0)}V_{13}^{(1)}\} -\Gamma_{3322}\rho_{22}^{(1)}-\Gamma_{3333}\rho_{33}^{(1)},$$

$$\frac{d\rho_{12}^{(1)}}{dt}=-\frac{i}{\hbar}\{(E_1-E_2)\rho_{12}^{(1)}+V_{12}^{(0)}(\rho_{22}^{(1)}-\rho_{11}^{(1)})+V_{13}^{(0)}\rho_{32}^{(1)} + V_{13}^{(1)}\rho_{32}^{(0)}\}-\Gamma_{1212}\rho_{12}^{(1)},$$

$$\frac{d\rho_{13}^{(1)}}{dt}=-\frac{i}{\hbar}\{(E_1-E_3)\rho_{13}^{(1)}+V_{13}^{(0)}(\rho_{33}^{(1)}-\rho_{11}^{(1)})+V_{12}^{(0)}\rho_{23}^{(1)} + V_{13}^{(1)}(\rho_{33}^{(0)}-\rho_{11}^{(0)})\}-\Gamma_{1313}\rho_{13}^{(1)},$$

$$\frac{d\rho_{23}^{(1)}}{dt}=-\frac{i}{\hbar}\{(E_2-E_3)\rho_{23}^{(1)}+V_{21}^{(0)}\rho_{13}^{(1)}-\rho_{21}^{(1)}V_{13}^{(0)}-\rho_{21}^{(0)}V_{13}^{(1)}\}$$
$$-\Gamma_{2323}\rho_{23}^{(1)}. \tag{3.3}$$

The probability conservation to first-order contributions implies now

$$\sum_{i=1}^{3}\rho_{ii}^{(1)}(t)=0. \tag{3.4}$$

Therefore, as done previously, we introduce the first-order terms of the population differences $\eta_{ij}^{(1)}=\rho_{ii}^{(1)}-\rho_{jj}^{(1)}$, which give in turn

$$\rho_{22}^{(1)}=\tfrac{2}{3}\eta_{21}^{(1)}-\tfrac{1}{3}\eta_{31}^{(1)},$$
$$\rho_{33}^{(1)}=\tfrac{2}{3}\eta_{31}^{(1)}-\tfrac{1}{3}\eta_{21}^{(1)}. \tag{3.5}$$

Also, we define the new first-order variables by the relations

$$\sigma_{12}^{(1)}=\rho_{12}^{(1)}\exp(-i\Omega_p t+i\mathbf{k}_p\cdot\mathbf{r}),$$
$$\sigma_{13}^{(1)}=\rho_{13}^{(1)}\exp(-i\Omega_t t+i\mathbf{k}_t\cdot\mathbf{r}),$$
$$\sigma_{23}^{(1)}=\rho_{23}^{(1)}\exp[i(\Omega_p-\Omega_t)t-i(\mathbf{k}_p-\mathbf{k}_t)\cdot\mathbf{r}],$$
$$\sigma_{ii}^{(1)}=\rho_{ii}^{(1)}\exp\forall i=1,2,3. \tag{3.6}$$

Finally, with these changes of variables and notations, the equation set (3.3) takes the form

$$\frac{\partial\eta_{21}^{(1)}}{\partial t}=2i\Omega_R(21,p)\sigma_{12}^{(1)}-2i\Omega_R(12,p)\sigma_{21}^{(1)}+i\Omega_R(31,t)\sigma_{13}^{(1)}$$
$$-i\Omega_R(13,t)\sigma_{31}^{(1)}+i\Omega_R(31,s)\exp[-i(\Omega_s-\Omega_t)t$$
$$+i(\mathbf{k}_s-\mathbf{k}_t)\cdot\mathbf{r}]\sigma_{13}^{(0)}-i\Omega_R(13,s)\exp[i(\Omega_s-\Omega_t)t$$
$$-i(\mathbf{k}_s-\mathbf{k}_t)\cdot\mathbf{r}]\sigma_{13}^{(0)}-\alpha_1\eta_{21}^{(1)}+\alpha_2\eta_{31}^{(1)},$$

$$\frac{\partial\eta_{31}^{(1)}}{\partial t}=2i\Omega_R(31,t)\sigma_{31}^{(1)}-2i\Omega_R(13,t)\sigma_{31}^{(1)}+i\Omega_R(21,p)\sigma_{12}^{(1)}$$
$$-i\Omega_R(12,p)\sigma_{21}^{(1)}+2i\Omega_R(31,s)\exp[-i(\Omega_s-\Omega_t)t$$
$$+i(\mathbf{k}_s-\mathbf{k}_t)\cdot\mathbf{r}]\sigma_{13}^{(0)}-2i\Omega_R(13,s)\exp[i(\Omega_s-\Omega_t)t$$
$$-i(\mathbf{k}_s-\mathbf{k}_t)\cdot\mathbf{r}]\sigma_{31}^{(0)}-\beta_1\eta_{31}^{(1)}+\beta_2\eta_{21}^{(1)},$$

$$\frac{\partial\sigma_{12}^{(1)}}{\partial t}=(i\omega_{21}-i\Omega_p+ik_{pz}v_z-\Gamma_{1212})\sigma_{12}^{(1)}+i\Omega_R(12,p)\eta_{21}^{(1)}$$
$$+i\Omega_R(13,t)\sigma_{32}^{(1)}+i\Omega_R(13,s)\exp[i(\Omega_s-\Omega_t)t$$
$$-i(\mathbf{k}_s-\mathbf{k}_t)\cdot\mathbf{r}]\sigma_{32}^{(0)},$$

$$\frac{\partial\sigma_{13}^{(1)}}{\partial t}+v_z\frac{\partial\sigma_{13}^{(1)}}{\partial z}=(i\omega_{31}-i\Omega_t+ik_{tz}v_z-\Gamma_{1313})\sigma_{13}^{(1)}$$
$$+i\Omega_R(12,p)\sigma_{23}^{(1)}+i\Omega_R(13,t)\eta_{31}^{(1)}$$
$$+i\Omega_R(13,s)\exp[i(\Omega_s-\Omega_t)t$$
$$-i(\mathbf{k}_s-\mathbf{k}_t)\cdot\mathbf{r}]\eta_{31}^{(0)},$$

$$\frac{\partial\sigma_{23}^{(1)}}{\partial t}+v_z\frac{\partial\sigma_{23}^{(1)}}{\partial z}=(i\omega_{32}+i\Omega_p-i\Omega_t-ik_{pz}v_z+ik_{tz}v_z$$
$$-\Gamma_{2323})\sigma_{23}^{(1)}+i\Omega_R(21,p)\sigma_{13}^{(1)}$$
$$-i\Omega_R(13,t)\sigma_{21}^{(1)}-i\Omega_R(13,s)\exp[i(\Omega_s$$
$$-\Omega_t)t-i(\mathbf{k}_s-\mathbf{k}_t)\cdot\mathbf{r}]\sigma_{21}^{(0)}, \tag{3.7}$$

where the rotating-wave approximation has been used. As previously mentioned, the Rabi frequencies are assumed real. Because of our variable change, we are left with a set of differential equations with coefficients oscillating at a single frequency and single wave vector. Then, a double Fourier series expansion in terms of this single frequency $\Delta_\Omega=\Omega_s-\Omega_t$ and wave vector $\mathbf{\Delta}_k=\mathbf{k}_s-\mathbf{k}_t$ can be introduced for the first-order population differences as well as for the coherences into the form

$$u^{(1)}(\mathbf{r},t)=\sum_{r=-\infty}^{\infty}\sum_{q=-\infty}^{\infty}u^{(1)(r,q)}(\Delta_\Omega,\mathbf{\Delta}_k)$$
$$\times\exp(ir\Delta_\Omega t+iq\mathbf{\Delta}_k\cdot\mathbf{r}). \tag{3.8}$$

Finally, owing to the real and imaginary parts of the coherences, as done for the zero-order contributions, we get

$$0=-4\Omega_R(21,p)\sigma_{\mathrm{Im}\,12}^{(1)(r,q)}(\Delta_\Omega,\mathbf{\Delta}_k)-2\Omega_R(31,t)\sigma_{\mathrm{Im}\,13}^{(1)(r,q)}$$
$$\times(\Delta_\Omega,\mathbf{\Delta}_k)-(ir\Delta_\Omega+\alpha_1)\eta_{21}^{(1)(r,q)}(\Delta_\Omega,\mathbf{\Delta}_k)+\alpha_2\eta_{31}^{(1)(r,q)}$$
$$\times(\Delta_\Omega,\mathbf{\Delta}_k)+i\Omega_R(31,s)\sigma_{13}^{(0)}\delta_{r,-1}\delta_{q,1}$$
$$-i\Omega_R(13,s)\sigma_{31}^{(0)}\delta_{r,1}\delta_{q,-1},$$

$$0=-4\Omega_R(31,t)\sigma_{\mathrm{Im}\,13}^{(1)(r,q)}(\Delta_\Omega,\mathbf{\Delta}_k)-2\Omega_R(21,p)\sigma_{\mathrm{Im}\,12}^{(1)(r,q)}$$
$$\times(\Delta_\Omega,\mathbf{\Delta}_k)-(ir\Delta_\Omega+\beta_1)\eta_{31}^{(1)(r,q)}(\Delta_\Omega,\mathbf{\Delta}_k)+\beta_2\eta_{21}^{(1)(r,q)}$$
$$\times(\Delta_\Omega,\mathbf{\Delta}_k)+2i\Omega_R(31,s)\sigma_{13}^{(0)}\delta_{r,-1}\delta_{q,1}$$
$$-2i\Omega_R(13,s)\sigma_{31}^{(0)}\delta_{r,1}\delta_{q,-1},$$

$$0=(-ir\Delta_\Omega-\Gamma_{1212})\sigma_{\mathrm{Re}\,12}^{(1)(r,q)}(\Delta_\Omega,\mathbf{\Delta}_k)-(\omega_{21}-\Omega_p$$
$$+k_{pz}v_z)\sigma_{\mathrm{Im}\,12}^{(1)(r,q)}(\Delta_\Omega,\mathbf{\Delta}_k)+\Omega_R(13,t)\sigma_{\mathrm{Im}\,23}^{(1)(r,q)}(\Delta_\Omega,\mathbf{\Delta}_k)$$
$$+\frac{i}{2}\Omega_R(13,s)\delta_{r,1}\delta_{q,-1}\sigma_{32}^{(0)}-\frac{i}{2}\Omega_R(13,s)\delta_{r,-1}\delta_{q,1}\sigma_{23}^{(0)},$$

$$0=(-ir\Delta_\Omega-\Gamma_{1212})\sigma_{\mathrm{Im}\,12}^{(1)(r,q)}(\Delta_\Omega,\mathbf{\Delta}_k)+(\omega_{21}-\Omega_p+k_{pz}v_z)\sigma_{\mathrm{Re}\,12}^{(1)(r,q)}(\Delta_\Omega,\mathbf{\Delta}_k)+\Omega_R(12,p)\,\eta_{21}^{(1)(r,q)}(\Delta_\Omega,\mathbf{\Delta}_k)+\Omega_R(13,t)\sigma_{\mathrm{Re}\,23}^{(1)(r,q)}(\Delta_\Omega,\mathbf{\Delta}_k)+\tfrac{1}{2}\Omega_R(13,s)\,\delta_{r,1}\delta_{q,-1}\sigma_{32}^{(0)}+\tfrac{1}{2}\Omega_R(13,s)\,\delta_{r,-1}\delta_{q,1}\sigma_{23}^{(0)},$$

$$0=(-ir\Delta_\Omega-iq\Delta_{kz}v_z-\Gamma_{1313})\sigma_{\mathrm{Re}\,13}^{(1)(r,q)}(\Delta_\Omega,\mathbf{\Delta}_k)-(\omega_{31}-\Omega_t+k_{tz}v_z)\sigma_{\mathrm{Im}\,13}^{(1)(r,q)}(\Delta_\Omega,\mathbf{\Delta}_k)-\Omega_R(12,p)\sigma_{\mathrm{Im}\,23}^{(1)(r,q)}(\Delta_\Omega,\mathbf{\Delta}_k)+\frac{i}{2}\Omega_R(13,s)[\,\delta_{r,1}\delta_{q,-1}-\delta_{r,-1}\delta_{q,1}]\,\eta_{31}^{(0)},$$

$$0=(-ir\Delta_\Omega-iq\Delta_{kz}v_z-\Gamma_{1313})\sigma_{\mathrm{Im}\,13}^{(1,q)(r)}(\Delta_\Omega,\mathbf{\Delta}_k)+(\omega_{31}-\Omega_t+k_{tz}v_z)\sigma_{\mathrm{Re}\,13}^{(1)(r,q)}(\Delta_\Omega,\mathbf{\Delta}_k)+\Omega_R(12,p)\sigma_{\mathrm{Re}\,23}^{(1)(r,q)}(\Delta_\Omega,\mathbf{\Delta}_k)+\Omega_R(13,t)\,\eta_{\mathrm{Re}\,31}^{(1)(r,q)}(\Delta_\Omega,\mathbf{\Delta}_k)+\tfrac{1}{2}\Omega_R(13,s)[\,\delta_{r,1}\delta_{q,-1}+\delta_{r,-1}\delta_{q,1}]\,\eta_{31}^{(0)},$$

$$0=(-ir\Delta_\Omega-iq\Delta_{kz}v_z-\Gamma_{2323})\sigma_{\mathrm{Re}\,23}^{(1)(r,q)}(\Delta_\Omega,\mathbf{\Delta}_k)-(\omega_{32}+\Omega_p-\Omega_t-k_{pz}v_z+k_{tz}v_z)\sigma_{\mathrm{Im}\,23}^{(1)(r,q)}(\Delta_\Omega,\mathbf{\Delta}_k)-\Omega_R(21,p)\sigma_{\mathrm{Im}\,13}^{(1)(r,q)}(\Delta_\Omega,\mathbf{\Delta}_k)-\Omega_R(13,t)\times\sigma_{\mathrm{Im}\,12}^{(1)(r,q)}(\Delta_\Omega,\mathbf{\Delta}_k)-\frac{i}{2}\Omega_R(13,s)[\,\delta_{r,1}\delta_{q,-1}\sigma_{21}^{(0)}-\delta_{r,-1}\delta_{q,1}\sigma_{12}^{(0)}],$$

$$0=(-ir\Delta_\Omega-iq\Delta_{kz}v_z-\Gamma_{2323})\sigma_{\mathrm{Im}\,23}^{(1)(r,q)}(\Delta_\Omega,\mathbf{\Delta}_k)+(\omega_{32}+\Omega_p-\Omega_t-k_{pz}v_z+k_{tz}v_z)\sigma_{\mathrm{Re}\,23}^{(1)(r,q)}(\Delta_\Omega,\mathbf{\Delta}_k)+\Omega_R(21,p)\sigma_{\mathrm{Re}\,13}^{(1)(r,q)}(\Delta_\Omega,\mathbf{\Delta}_k)-\Omega_R(13,t)\times\sigma_{\mathrm{Re}\,12}^{(1)(r,q)}(\Delta_\Omega,\mathbf{\Delta}_k)-\tfrac{1}{2}\Omega_R(13,s)[\,\delta_{r,1}\delta_{q,-1}\sigma_{21}^{(0)}+\delta_{r,-1}\delta_{q,1}\sigma_{12}^{(0)}],\tag{3.9}$$

if we remember that to zero-order, implying the V system and the two strong beams, the population differences $\eta_{ij}^{(0)}$ and the coherences $\sigma_{ij}^{(0)}$ are not depending on time. Of course, the density matrix elements $\rho_{ij}^{(0)}$ are time dependent. As usual this equation set can be recast into a matrix form. It gives

$$W^{(r,q)}(\Delta_\Omega,\mathbf{\Delta}_k)\mathbf{\Sigma}^{(1)(r,q)}(\Delta_\Omega,\mathbf{\Delta}_k)=\Omega_R(13,s)[\,\mathbf{\Lambda}_{r,q}\delta_{r,1}\delta_{q,-1}+\mathbf{\Lambda}_{r,q}\delta_{r,-1}\delta_{q,1}],\tag{3.10}$$

where the vector $\mathbf{\Sigma}^{(1)(r,q)}(\Delta_\Omega,\mathbf{\Delta}_k)$ is built up from the first-order Fourier components as:

$$\mathbf{\Sigma}^{(1)(r,q)}=\{\eta_{21}^{(1)(r,q)},\eta_{31}^{(1)(r,q)},\sigma_{\mathrm{Re}\,12}^{(1)(r,q)},\sigma_{\mathrm{Im}\,12}^{(1)(r,q)},\sigma_{\mathrm{Re}\,13}^{(1)(r,q)},\sigma_{\mathrm{Im}\,13}^{(1)(r,q)},\sigma_{\mathrm{Re}\,23}^{(1)(r,q)},\sigma_{\mathrm{Im}\,23}^{(1)(r,q)}\},\tag{3.11}$$

where, for the sake of simplicity, the $\Delta_\Omega$ and $\mathbf{\Delta}_k$ dependences have been omitted in the components. Also, the other two vectors $\mathbf{\Lambda}_{1,-1}$ and $\mathbf{\Lambda}_{-1,1}$ can be expressed with the relations $\sigma_{\mathrm{Re}\,ij}^{(0)}=\sigma_{\mathrm{Re}\,ji}^{(0)}$ and $\sigma_{\mathrm{Im}\,ij}^{(0)}=-\sigma_{\mathrm{Im}\,ji}^{(0)}$ in the form

$$\mathbf{\Lambda}_{1,-1}=\left\{i\sigma_{31}^{(0)},2i\sigma_{31}^{(0)},-\frac{i}{2}\sigma_{32}^{(0)},-\frac{1}{2}\sigma_{32}^{(0)},-\frac{i}{2}\eta_{31}^{(0)},-\frac{1}{2}\eta_{31}^{(0)},\frac{i}{2}\sigma_{21}^{(0)},\frac{1}{2}\sigma_{21}^{(0)}\right\},$$

$$\mathbf{\Lambda}_{-1,1}=\left\{-i\sigma_{13}^{(0)},-2i\sigma_{13}^{(0)},\frac{i}{2}\sigma_{23}^{(0)},-\frac{1}{2}\sigma_{23}^{(0)},\frac{i}{2}\eta_{31}^{(0)},-\frac{1}{2}\eta_{31}^{(0)},-\frac{i}{2}\sigma_{12}^{(0)},\frac{1}{2}\sigma_{12}^{(0)}\right\},\tag{3.12}$$

by using the simplifying notation previously introduced. Finally, the matrix $W^{(r,q)}$ corresponds to

$$W^{(r,q)}=\begin{pmatrix}W_1^{(r,q)} & W_2^{(r,q)}\\ W_3^{(r,q)} & W_4^{(r,q)}\end{pmatrix},\tag{3.13}$$

where the various submatrices $W_j^{(r,q)}$ with $j=1-4$ correspond to

$$W_1^{(r,q)}=\begin{pmatrix} ir\Delta_\Omega-\alpha_1 & \alpha_2 & 0 & -4\Omega_R(21,p) \\ \beta_2 & -ir\Delta_\Omega-\beta_1 & 0 & -2\Omega_R(21,p) \\ 0 & 0 & -ir\Delta_\Omega-\Gamma_{1212} & -\omega_{21}+\Omega_p' \\ \Omega_R(12,p) & 0 & \omega_{21}-\Omega_p' & -ir\Delta_\Omega-\Gamma_{1212} \end{pmatrix},$$

$$W_2^{(r,q)}=\begin{pmatrix} 0 & -2\Omega_R(31,t) & 0 & 0 \\ 0 & -4\Omega_R(31,t) & 0 & 0 \\ 0 & 0 & 0 & \Omega_R(13,t) \\ 0 & 0 & \Omega_R(13,t) & 0 \end{pmatrix},$$

$$W_3^{(r,q)}=\begin{pmatrix} 0 & 0 & 0 & 0 \\ 0 & \Omega_R(13,t) & 0 & 0 \\ 0 & 0 & 0 & -\Omega_R(13,t) \\ 0 & 0 & -\Omega_R(13,t) & 0 \end{pmatrix},$$

$$W_4^{(r,q)}=\begin{pmatrix} -ir\Delta_\Omega-iq\Delta_k-\Gamma_{1313} & -\omega_{31}+\Omega_t' & 0 & -\Omega_R(12,p) \\ \omega_{31}-\Omega_t' & -ir\Delta_\Omega-iq\Delta_k-\Gamma_{1313} & \Omega_R(12,p) & 0 \\ 0 & -\Omega_R(21,p) & -ir\Delta_\Omega-iq\Delta_k-\Gamma_{2323} & -\omega_{32}-\Omega_p'+\Omega_t' \\ \Omega_R(12,p) & 0 & \omega_{32}+\Omega_p'-\Omega_t' & -ir\Delta_\Omega-iq\Delta_k-\Gamma_{2323} \end{pmatrix}. \quad (3.14)$$

From Eq. (3.10), the solution can easily been obtained from simple algebra. First, the equation has to be solved for the Fourier component $r=0$ as indicated in the preceding section to get the vectors $\mathbf{\Lambda}_{1,-1}$ and $\mathbf{\Lambda}_{-1,1}$. Next, the Fourier components $\mathbf{\Sigma}^{(1)(1,-1)}$ and $\mathbf{\Sigma}^{(1)(-1,1)}$ can be determined along the same lines. Of course, from the homogeneous system obtained for the other combinations of $(r,q)$, we conclude that their Fourier components cancel identically. From the structure of Eq. (3.10), the contribution to the polarization in the direction $\mathbf{k}_s$ of the probe beam is obtained straightforwardly. The general expression of the $\mathbf{k}_s$ component of the polarization takes the form

$$\mathbf{P}^{(1)}(\mathbf{k}_s,\Omega_s,t)=\rho_{13}^{(1)}(\mathbf{k}_s,\Omega_s,t)\boldsymbol{\mu}_{31}+\rho_{31}^{(1)}(\mathbf{k}_s,\Omega_s,t)\boldsymbol{\mu}_{13}\approx\sigma_{13}^{(1)(1,-1)}(\Delta_\Omega,\mathbf{\Delta}_k)\boldsymbol{\mu}_{31}\exp(i\Omega_s t-i\mathbf{k}_s\cdot\mathbf{r}), \quad (3.15)$$

if we reject highly oscillating terms whose contributions are negligible. From our calculation, it can be put into an explicit form as

$$\mathbf{P}^{(1)}(\mathbf{k}_s,\Omega_s,t)=\boldsymbol{\mu}_{31}\Omega_R(13,s)e^{i\Omega_s t-i\mathbf{k}_s\cdot\mathbf{r}}\frac{1}{\det W^{(1,-1)}}\left\{\begin{vmatrix} \cdots & \Lambda_{1,-1(1)} & \cdots \\ \cdots & \Lambda_{1,-1(2)} & \cdots \\ \cdots & \Lambda_{1,-1(3)} & \cdots \\ \vdots\vdots & \vdots & \vdots\vdots \\ \cdots & \Lambda_{1,-1(7)} & \cdots \\ \cdots & \Lambda_{1,-1(8)} & \cdots \end{vmatrix}+i\begin{vmatrix} \cdots & \Lambda_{1,-1(1)} & \cdots \\ \cdots & \Lambda_{1,-1(2)} & \cdots \\ \cdots & \Lambda_{1,-1(3)} & \cdots \\ \vdots\vdots & \vdots & \vdots\vdots \\ \cdots & \Lambda_{1,-1(7)} & \cdots \\ \cdots & \Lambda_{1,-1(8)} & \cdots \end{vmatrix}\right\}. \quad (3.16)$$

Notice that all the dots in the determinants correspond to the matrix elements taken from matrix (3.13) for the corresponding values of $r$ and $q$, and that the values $\Lambda_{r,q(j)}$ are the components of vectors $\mathbf{\Lambda}_{1,-1}$. If we are interested in the determination of the integrated signal obtained experimentally, we have

$$I(\mathbf{k}_s,\Omega_s)=\frac{1}{T}\int_{-T/2}^{T/2}dt|\mathbf{P}^{(1)}(\mathbf{k}_s,\Omega_s,t)|^2. \quad (3.17)$$

This quantity will be the starting point of a number of numerical simulations to illustrate the influence of the various dynamical constants on the TC-RFWM spectra.

To emphasize these analytical results, as well as the influence of the various physical processes on the TC-RFWM spectra, we will present some numerical simulations. Their implementation is realized by using formal algebra to avoid the explicit development of the determinants. Otherwise, the evaluation is straightforwardly done. All along, the geometry will be defined by the angle between the wave vector $\mathbf{k}_p$ and

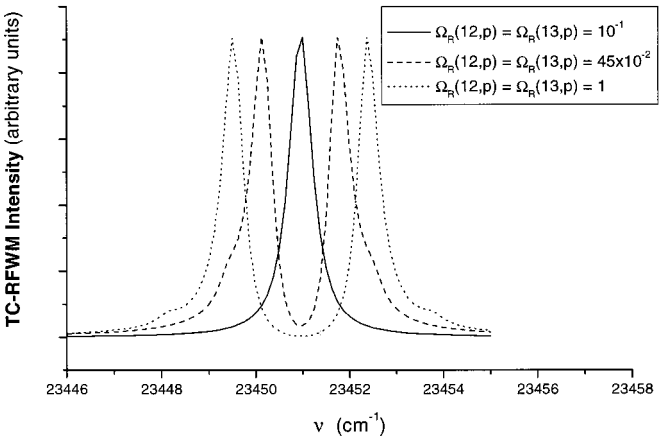


FIG. 3. We exhibit the probe field frequency dependence of the TC-RFWM spectra for various values of the Rabi frequencies chosen equal for the grating beams so that $\Omega_R(12,p)=\Omega_R(13,t)$ in the GSG spectroscopy. The values of the Rabi frequencies for the grating beams are indicated in the inset. Other values are for the transition and field frequencies $\omega_{31}=\Omega_t=23\,460.96\ \mathrm{cm}^{-1}$, $\omega_{21}=\Omega_p=25\,818.90\ \mathrm{cm}^{-1}$, for the total decay rates $\Gamma_{2222}=\Gamma_{3333}=0.35\ \mathrm{cm}^{-1}$, for the transition constant $\Gamma_{2233}=0$, for the pure dephasing constants $\Gamma_{ijij}^{(d)}=0\ \forall\ (i,j)$, for the probe Rabi frequency $\Omega_R(12,s)=0.005\ \mathrm{cm}^{-1}$, and finally for the transverse velocity $v_z=0$.

$\mathbf{k}_t$ of the grating fields and the $z$ axis. They correspond to $\theta_p=-\theta_t=-\pi/180$ rad, respectively. The probe beam is counterpropagating along the $z$ axis so that $\phi=\pi$ rad. For the present model of two beams acting on two different transitions sharing a common level, we first analyze the influence of the grating field amplitudes chosen equal for simplicity. The variations are represented on Fig. 3, where the various spectra have been normalized. When the grating field amplitudes $E_p(\Omega_p)$ and $E_t(\Omega_t)$ increase, the true states experimentally accessible are the dressed molecular states resulting from the diagonalization of the radiation-matter interaction in the zero-order field and molecule states [36]. When the grating field amplitudes are strong enough, the transitions between dressed molecular states notably differ from those between the molecular states and we observe a line splitting of the molecular resonance. As long as the molecular velocity is neglected, the TC-RFWM spectra is symmetric [29]. Here, because the spectra is observed in the frequency range of the 1-3 transition frequency, the main feature consists of two lines resulting from the line splitting of the 1-3 resonance. However, we really have a three-level system and the diagonalization has to be done in the full space. This implies additional molecular dressed states with respect to the two-level system. Consequently, transitions between these dressed states give rise to additional resonances, which appear on the shoulder of the spectrum obtained for $\Omega_R(12,p)=\Omega_R(13,t)=1$. Of course, their contributions are small due to their nonresonant excitation. Next, we analyze in Fig. 4 the role played by the transition constants $\Gamma_{2233}$ and $\Gamma_{3322}$. These constants result from the coupling between the two configurations involving the molecular states $|1\rangle$ or $|3\rangle$ associated with a manifold of bath states. Of course, according to the bath temperature, we have a distribution population effect between these configurations, which is accounted for by the well-known detailed balance equation $\Gamma_{3322}=\exp(-\hbar\omega_{32}/kT)\Gamma_{2233}$ between direct and reverse transition constants. As expected, for increasing values of $\Gamma_{2233}$, we note a strong reduction of the dip due to the rapid transfer between the levels 2 and 3. For higher values of $\Gamma_{2233}$, the spectrum will look like to a single resonance with a shape strongly temperature dependent through the coefficient $\exp(-\hbar\omega_{32}/kT)$ relating the transition constants $\Gamma_{3322}$ and $\Gamma_{2233}$.

Of course, at very low grating field intensities, the dynamical equation corresponds to the linearization of the Liouville equation (3.2) with respect to the grating field amplitudes and we recover all the results previously established in the low-field regime.

## IV. DYNAMICS INDUCED BY A BICHROMATIC FIELD AND PROBED ON A DIFFERENT TRANSITION

In the present section, we consider the case of a V or $\Lambda$ system with one side driven by a bichromatic field, while the other one is tested by a weak probe field, as shown in Fig. 5. Again, like in the preceding section, we will emphasize more on the V structure but, as previously mentioned, with small changes the other situation can be handled as well. The bichromatic field responsible for the diffraction grating and the probing field are described by their corresponding electric fields

$$\mathbf{E}_p(\mathbf{r},t)=\mathbf{E}_p(\Omega_p)\exp[-i(\Omega_p t-\mathbf{k}_p\cdot\mathbf{r})][1+\alpha e^{-i\mathbf{\Delta}_k\cdot\mathbf{r}}]+\text{c.c.},$$

$$\mathbf{E}_s(\mathbf{r},t)=\mathbf{E}_s(\Omega_s)\exp[-i(\Omega_s t-\mathbf{k}_s\cdot\mathbf{r})]+\text{c.c.} \qquad (4.1)$$

by using the same notations previously introduced. Here, the quantity $\mathbf{E}_s(\Omega_s)$ stands for the amplitude of the probe field with wave vector $\mathbf{k}_s$, and $\mathbf{E}_p(\Omega_p)$ and $\alpha\mathbf{E}_p(\Omega_p)$ are the amplitudes for the bichromatic field associated with the wave vectors $\mathbf{k}_p$ and $\mathbf{k}_p-\mathbf{\Delta}_k$, respectively. The dynamical evolution induced by the grating beam applied on the $|1\rangle\rightarrow|2\rangle$ transition, and the probing beam acting on the $|1\rangle\rightarrow|3\rangle$ transition, is again introduced by using the rotating-wave approximation. This basic description of bichromatic fields acting on a three-level system has been done for a large number of problems as different as coherent effects in the V model [9], light pressure forces in intense polychromatic fields [11,37], or multiphoton Raman resonances in $\Lambda$ atoms [12]. The evolution of the populations and coherences corresponds to

$$\frac{d\rho_{22}}{dt}=\left[-\frac{i}{\hbar}\boldsymbol{\mu}_{12}\cdot\mathbf{E}_p(\Omega_p)\exp[i(\Omega_p t-\mathbf{k}_p\cdot\mathbf{r})][1+\alpha e^{-i\mathbf{\Delta}_k\cdot\mathbf{r}}]\times\rho_{21}+\text{c.c.}\right]-\Gamma_{2211}\rho_{11}-\Gamma_{2222}\rho_{22}-\Gamma_{2233}\rho_{33},$$

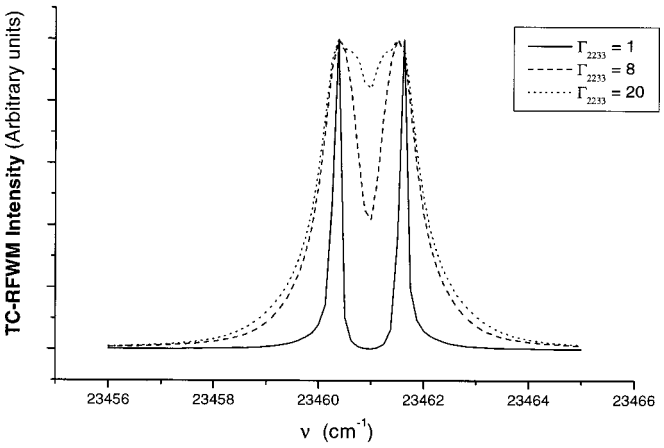


FIG. 4. We represent the influence of the nonradiative processes taking place between levels 2 and 3 on the TC-RFWM spectra obtained from GSG spectroscopy. The probe frequency dependence is drawn for the three different values of $\Gamma_{2233}$ indicated in the inset. The Rabi frequencies for the grating beams are $\Omega_R(12,p)=\Omega_R(13,t)=0.45\ \mathrm{cm}^{-1}$, $kT/\omega_{32}=0.05$, all the other values being kept identical to those of Fig. 3.

$$\frac{d\rho_{33}}{dt}=\left[-\frac{i}{\hbar}\boldsymbol{\mu}_{13}\cdot\mathbf{E}_s(\Omega_s)\exp[i(\Omega_s t-\mathbf{k}_s\cdot\mathbf{r})]\rho_{31}+\text{c.c.}\right]-\Gamma_{3311}\rho_{11}-\Gamma_{3322}\rho_{22}-\Gamma_{3333}\rho_{33},$$

$$\frac{d\rho_{12}}{dt}=[i\omega_{21}-\Gamma_{1212}]\rho_{12}+\frac{i}{\hbar}\boldsymbol{\mu}_{12}\cdot\mathbf{E}_p(\Omega_p)\times\exp[i(\Omega_p t-\mathbf{k}_p\cdot\mathbf{r})][1+\alpha e^{-i\boldsymbol{\Delta}_k\cdot\mathbf{r}}][\rho_{22}-\rho_{11}]+\frac{i}{\hbar}\boldsymbol{\mu}_{13}\cdot\mathbf{E}_s(\Omega_s)\exp[i(\Omega_s t-\mathbf{k}_s\cdot\mathbf{r})]\rho_{32},$$

$$\frac{d\rho_{13}}{dt}=[i\omega_{31}-\Gamma_{1313}]\rho_{13}+\frac{i}{\hbar}\boldsymbol{\mu}_{12}\cdot\mathbf{E}_p(\Omega_p)\times\exp[i(\Omega_p t-\mathbf{k}_p\cdot\mathbf{r})][1+\alpha e^{-i\boldsymbol{\Delta}_k\cdot\mathbf{r}}]\rho_{23}+\frac{i}{\hbar}\boldsymbol{\mu}_{13}\cdot\mathbf{E}_s(\Omega_s)\exp[i(\Omega_s t-\mathbf{k}_s\cdot\mathbf{r})][\rho_{33}-\rho_{11}],$$

$$\frac{d\rho_{23}}{dt}=[i\omega_{32}-\Gamma_{2323}]\rho_{23}+\frac{i}{\hbar}\boldsymbol{\mu}_{21}\cdot\mathbf{E}_p^*(\Omega_p)\times\exp[-i(\Omega_p t-\mathbf{k}_p\cdot\mathbf{r})][1+\alpha^* e^{i\boldsymbol{\Delta}_k\cdot\mathbf{r}}]\rho_{13}-\frac{i}{\hbar}\rho_{21}\boldsymbol{\mu}_{13}\cdot\mathbf{E}_s(\Omega_s)\exp[i(\Omega_s t-\mathbf{k}_s\cdot\mathbf{r})],\quad(4.2)$$

where the definition of the time derivative and the assumptions (2.3) are still valid. For the present purpose, it is convenient to introduce the change of variables

$$\rho_{21}=e^{-i\Omega_p t}[s_p e^{i\mathbf{k}_p\cdot\mathbf{r}}+r_p e^{-i\mathbf{k}_p\cdot\mathbf{r}}],$$

$$\rho_{31}=e^{-i\Omega_s t}[s_s e^{i\mathbf{k}_s\cdot\mathbf{r}}+r_s e^{-i\mathbf{k}_s\cdot\mathbf{r}}],$$

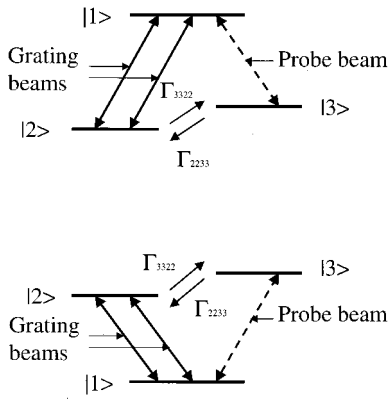


FIG. 5. Energetic level structures analogous to those previously shown in Fig. 2, except for the grating beams, which act, here, on the same transition.

$$\rho_{23}=e^{-i(\Omega_p-\Omega_s)t}[s_-\exp[-i(\mathbf{k}_p-\mathbf{k}_s)\cdot\mathbf{r}]+r_-\exp[i(\mathbf{k}_p-\mathbf{k}_s)\cdot\mathbf{r}]+s_+\exp[i(\mathbf{k}_p+\mathbf{k}_s)\cdot\mathbf{r}]+r_+\exp[-i(\mathbf{k}_p+\mathbf{k}_s)\cdot\mathbf{r}]].\quad(4.3)$$

From the set of equations (4.2), by identifying the various **k** components, we get for the coherences

$$\dot{s}_p^*=[i(\omega_{21}-\Omega_p+k_{pz}v_z)-\Gamma_{1212}]s_p^*+\frac{i}{\hbar}\boldsymbol{\mu}_{12}\cdot\mathbf{E}_p(\Omega_p)\times[1+\alpha e^{-i\boldsymbol{\Delta}_k\cdot\mathbf{r}}](\rho_{22}-\rho_{11})+\frac{i}{\hbar}\boldsymbol{\mu}_{13}\cdot\mathbf{E}_s(\Omega_s)r_-^*,$$

$$\dot{r}_p^*=[i(\omega_{21}-\Omega_p-k_{pz}v_z)-\Gamma_{1212}]r_p^*+\frac{i}{\hbar}\boldsymbol{\mu}_{13}\cdot\mathbf{E}_s(\Omega_s)r_+^*,$$

$$\dot{s}_s^*=[i(\omega_{31}-\Omega_s+k_{sz}v_z)-\Gamma_{1313}]s_s^*+\frac{i}{\hbar}\boldsymbol{\mu}_{12}\cdot\mathbf{E}_p(\Omega_p)r_-+\frac{i}{\hbar}\boldsymbol{\mu}_{13}\cdot\mathbf{E}_s(\Omega_s)(\rho_{33}-\rho_{11}),$$

$$\dot{r}_s^*=[i(\omega_{31}-\Omega_s-k_{sz}v_z)-\Gamma_{1313}]r_s^*+\frac{i}{\hbar}\boldsymbol{\mu}_{12}\cdot\mathbf{E}_p(\Omega_p)s_+,$$

$$\dot{r}_-=[i\{\omega_{32}+\Omega_p-\Omega_s-(k_{pz}-k_{sz})v_z\}-\Gamma_{2323}]r_-+\frac{i}{\hbar}\boldsymbol{\mu}_{21}\cdot\mathbf{E}_p^*(\Omega_p)[1+\alpha^* e^{i\boldsymbol{\Delta}_k\cdot\mathbf{r}}]s_s^*-\frac{i}{\hbar}\boldsymbol{\mu}_{13}\cdot\mathbf{E}_s(\Omega_s)s_p,$$

$$\dot{s}_+=[i\{\omega_{32}+\Omega_p-\Omega_s-(k_{pz}+k_{sz})v_z\}-\Gamma_{2323}]s_+ +\frac{i}{\hbar}\boldsymbol{\mu}_{21}\cdot\mathbf{E}_p^*(\Omega_p)[1+\alpha^* e^{i\boldsymbol{\Delta}_k\cdot\mathbf{r}}]r_s^*.\quad(4.4)$$

This equation set can be solved easily. Indeed, a quick examination of the fourth and sixth equalities shows that they constitute an homogeneous equation set, so that $r_s^*=s_+=0$. To solve the equation set for the remaining coefficients, we first need the solutions for the populations. If the probe

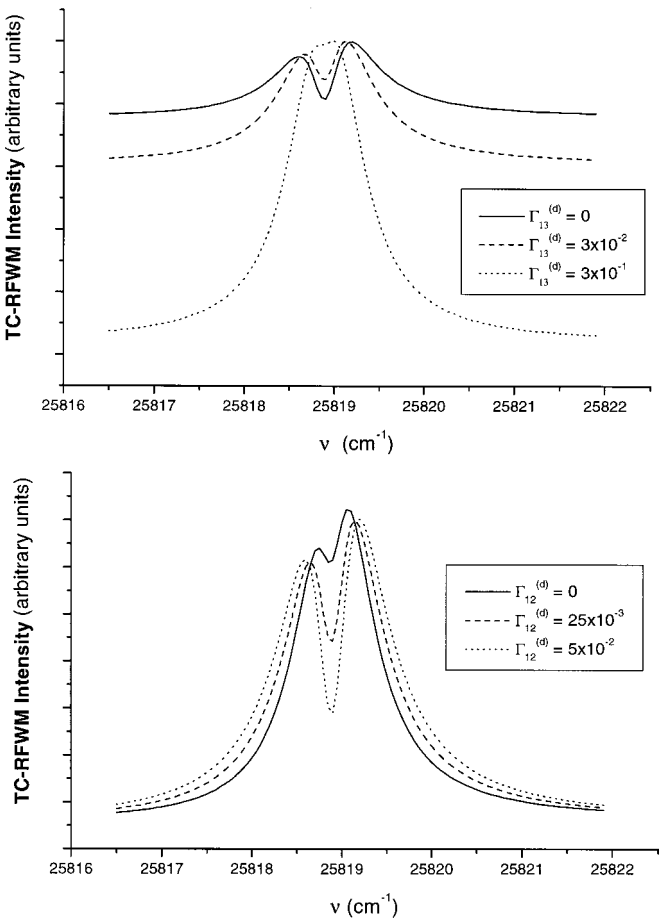


FIG. 6. Influence of the pure dephasing processes $\Gamma_{12}^{(d)}$ and $\Gamma_{13}^{(d)}$ on the grating beam frequency dependence of the TC-RFWM spectra. The basic difference comes from the fact that the transitions 1-2 and 1-3 are driven by a strong field and a weak field, respectively. The values of the pure dephasing constants are given on the insets and are equal to zero if not indicated. Other values are for the transition constant $\Gamma_{2233}=0$, for the Rabi frequencies $\Omega_R^{12}=0.075\ \text{cm}^{-1}$, $\Omega_R^{13}=0.005\ \text{cm}^{-1}$, for the transverse velocity $v_z=-1.4\times10^{-7}\ \text{cm s}^{-1}$ with $c$ the light velocity, and finally for the field parameters $\alpha=1$ and $x=1$. Other values are kept identical to those of Fig. 3.

field $\mathbf{E}_s(\mathbf{r},t)$ is weak enough, it suffices to calculate the populations to zero order on the probe beam and this approximation will be also true for the evaluation of the coefficient $s_p^*$ participating in the dynamical evolution of the populations. Therefore, if we remember that the population conservation requires $\Sigma_j\rho_{jj}=1$, we obtain

$$\dot{\rho}_{22}^{(0)}=\frac{i}{\hbar}\boldsymbol{\mu}_{21}\cdot\mathbf{E}_p^*(\Omega_p)[1+\alpha^* e^{i\boldsymbol{\Delta}_k\cdot\mathbf{r}}]s_p^{(0)*}-\frac{i}{\hbar}\boldsymbol{\mu}_{12}\cdot\mathbf{E}_p(\Omega_p)\times[1+\alpha e^{-i\boldsymbol{\Delta}_k\cdot\mathbf{r}}]s_p^{(0)}-\Gamma_{2222}\rho_{22}^{(0)}-\Gamma_{2233}\rho_{33}^{(0)},$$

$$\dot{\rho}_{33}^{(0)}=-\Gamma_{3333}\rho_{33}^{(0)}-\Gamma_{3322}\rho_{22}^{(0)},$$

$$\dot{s}_p^{(0)*}=[i(\omega_{21}-\Omega_p+k_{pz}v_z)-\Gamma_{1212}]s_p^{(0)*}+\frac{i}{\hbar}\boldsymbol{\mu}_{12}\cdot\mathbf{E}_p(\Omega_p)\times[1+\alpha e^{-i\boldsymbol{\Delta}_k\cdot\mathbf{r}}](2\rho_{22}^{(0)}+\rho_{33}^{(0)}-1). \quad (4.5)$$

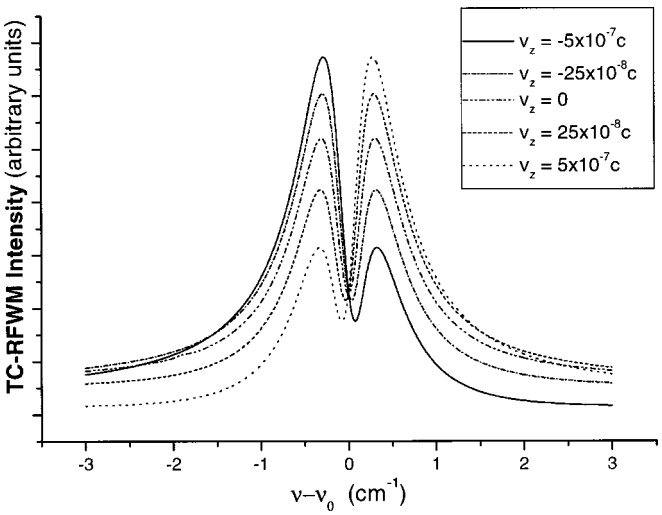


FIG. 7. We present the grating beam frequency dependence of the TC-RFWM spectra for different values of the transverse velocity indicated in the inset. The physical parameters are $\Gamma_{iiii}=0.35\ \text{cm}^{-1}$ for $i=2$, 3, $\Gamma_{12}^{(d)}=\Gamma_{13}^{(d)}=0$, $\Gamma_{2233}=0$, and finally $\Omega_R^{12}=0.085\ \text{cm}^{-1}$, $\Omega_R^{13}=0.005\ \text{cm}^{-1}$. Other values are identical to those of Fig. 6.

Introducing the Fourier series expansion

$$u(t)=\sum_{n=-\infty}^{+\infty}u^{(n)}(\omega)e^{in\omega t} \quad (4.6)$$

and the notation $s_p^{(0)}=s_{p(r)}^{(0)}+is_{p(i)}^{(0)}$ standing for the real and imaginary parts as well as $\Omega_R^{12}$ and $\Omega_R^{13}$ for the Rabi frequencies of the grating ($p$) and probe ($s$) fields, we get

$$in\omega\rho_{22}^{(0)(n)}(\omega)=-\Gamma_{2222}\rho_{22}^{(0)(n)}(\omega)-\Gamma_{3333}\rho_{33}^{(0)(n)}(\omega)+2\Omega_R^{12}[1+\alpha\cos(\boldsymbol{\Delta}_k\cdot\mathbf{r})]s_{p(i)}^{(0)(n)}(\omega)-2\Omega_R^{12}\alpha\sin(\boldsymbol{\Delta}_k\cdot\mathbf{r})s_{p(r)}^{(0)(n)}(\omega),$$

$$in\omega\rho_{33}^{(0)(n)}(\omega)=-\Gamma_{3333}\rho_{33}^{(0)(n)}(\omega)-\Gamma_{3322}\rho_{22}^{(0)(n)}(\omega),$$

$$in\omega s_{p(r)}^{(0)(n)}(\omega)=-\Gamma_{1212}s_{p(r)}^{(0)(n)}(\omega)+(\omega_{21}-\Omega_p+k_{pz}v_z)\times s_{p(i)}^{(0)(n)}(\omega)+2\Omega_R^{12}\alpha\sin(\boldsymbol{\Delta}_k\cdot\mathbf{r})[\rho_{22}^{(0)(n)}(\omega)+\rho_{33}^{(0)(n)}(\omega)]-\Omega_R^{12}\alpha\sin(\boldsymbol{\Delta}_k\cdot\mathbf{r}),$$

$$in\omega s_{p(i)}^{(0)(n)}(\omega)=-\Gamma_{1212}s_{p(i)}^{(0)(n)}(\omega)-(\omega_{21}-\Omega_p+k_{pz}v_z)\times s_{p(r)}^{(0)(n)}(\omega)-2\Omega_R^{12}[1+\alpha\cos(\boldsymbol{\Delta}_k\cdot\mathbf{r})]\times[\rho_{22}^{(0)(n)}(\omega)+\rho_{33}^{(0)(n)}(\omega)]+\Omega_R^{12}[1+\alpha\cos(\boldsymbol{\Delta}_k\cdot\mathbf{r})]. \quad (4.7)$$

The solutions are

$$\rho_{22}^{(0)(n)}(\omega)=\rho_{33}^{(0)(n)}(\omega)=s_{p(r)}^{(0)(n)}(\omega)=s_{p(i)}^{(0)(n)}(\omega)=0 \quad \text{for } n\neq0, \quad (4.8)$$

while for $n=0$, with the notation

$$\Delta(n)=\begin{vmatrix} -in\omega-\Gamma_{2222} & -\Gamma_{2233} & -2\Omega_R^{12}\alpha\sin(\mathbf{\Delta}_k\cdot\mathbf{r}) & 2\Omega_R^{12}[1+\alpha\cos(\mathbf{\Delta}_k\cdot\mathbf{r})] \\ -\Gamma_{3322} & -in\omega-\Gamma_{3333} & 0 & 0 \\ 2\Omega_R^{12}\alpha\sin(\mathbf{\Delta}_k\cdot\mathbf{r}) & \Omega_R^{12}\alpha\sin(\mathbf{\Delta}_k\cdot\mathbf{r}) & -in\omega-\Gamma_{1212} & \omega_{21}-\Omega_p+k_{pz}v_z \\ -2\Omega_R^{12}[1+\alpha\cos(\mathbf{\Delta}_k\cdot\mathbf{r})] & -\Omega_R^{12}[1+\alpha\cos(\mathbf{\Delta}_k\cdot\mathbf{r})] & -\omega_{21}+\Omega_p-k_{pz}v_z & -in\omega-\Gamma_{1212} \end{vmatrix}, \tag{4.9}$$

we have

$$\rho_{22}^{(0)(0)}(\omega)=\frac{1}{\Delta(0)}\begin{vmatrix} 0 & -\Gamma_{2233} & -2\Omega_R^{12}\alpha\sin(\mathbf{\Delta}_k\cdot\mathbf{r}) & 2\Omega_R^{12}[1+\alpha\cos(\mathbf{\Delta}_k\cdot\mathbf{r})] \\ 0 & -\Gamma_{3333} & 0 & 0 \\ \Omega_R^{12}\alpha\sin(\mathbf{\Delta}_k\cdot\mathbf{r}) & \Omega_R^{12}\alpha\sin(\mathbf{\Delta}_k\cdot\mathbf{r}) & -\Gamma_{1212} & \omega_{21}-\Omega_p+k_{pz}v_z \\ -\Omega_R^{12}[1+\alpha\cos(\mathbf{\Delta}_k\cdot\mathbf{r})] & -\Omega_R^{12}[1+\alpha\cos(\mathbf{\Delta}_k\cdot\mathbf{r})] & -\omega_{21}+\Omega_p-k_{pz}v_z & -\Gamma_{1212} \end{vmatrix},$$

$$\rho_{33}^{(0)(0)}(\omega)=\frac{1}{\Delta(0)}\begin{vmatrix} -\Gamma_{2222} & 0 & -2\Omega_R^{12}\alpha\sin(\mathbf{\Delta}_k\cdot\mathbf{r}) & 2\Omega_R^{12}[1+\alpha\cos(\mathbf{\Delta}_k\cdot\mathbf{r})] \\ -\Gamma_{3322} & 0 & 0 & 0 \\ 2\Omega_R^{12}\alpha\sin(\mathbf{\Delta}_k\cdot\mathbf{r}) & \Omega_R^{12}\alpha\sin(\mathbf{\Delta}_k\cdot\mathbf{r}) & -\Gamma_{1212} & \omega_{21}-\Omega_p+k_{pz}v_z \\ -2\Omega_R^{12}[1+\alpha\cos(\mathbf{\Delta}_k\cdot\mathbf{r})] & -\Omega_R^{12}[1+\alpha\cos(\mathbf{\Delta}_k\cdot\mathbf{r})] & -\omega_{21}+\Omega_p-k_{pz}v_z & -\Gamma_{1212} \end{vmatrix},$$

$$s_{p(r)}^{(0)(0)}(\omega)=\frac{1}{\Delta(0)}\begin{vmatrix} -\Gamma_{2222} & -\Gamma_{2233} & 0 & 2\Omega_R^{12}[1+\alpha\cos(\mathbf{\Delta}_k\cdot\mathbf{r})] \\ -\Gamma_{3322} & -\Gamma_{3333} & 0 & 0 \\ 2\Omega_R^{12}\alpha\sin(\mathbf{\Delta}_k\cdot\mathbf{r}) & \Omega_R^{12}\alpha\sin(\mathbf{\Delta}_k\cdot\mathbf{r}) & \Omega_R^{12}\alpha\sin(\mathbf{\Delta}_k\cdot\mathbf{r}) & \omega_{21}-\Omega_p+k_{pz}v_z \\ -2\Omega_R^{12}[1+\alpha\cos(\mathbf{\Delta}_k\cdot\mathbf{r})] & -\Omega_R^{12}[1+\alpha\cos(\mathbf{\Delta}_k\cdot\mathbf{r})] & -\Omega_R^{12}[1+\alpha\cos(\mathbf{\Delta}_k\cdot\mathbf{r})] & -\Gamma_{1212} \end{vmatrix},$$

$$s_{p(i)}^{(0)(0)}(\omega)=\frac{1}{\Delta(0)}\begin{vmatrix} -\Gamma_{2222} & -\Gamma_{2233} & -2\Omega_R^{12}\alpha\sin(\mathbf{\Delta}_k\cdot\mathbf{r}) & 0 \\ -\Gamma_{3322} & -\Gamma_{3333} & 0 & 0 \\ 2\Omega_R^{12}\alpha\sin(\mathbf{\Delta}_k\cdot\mathbf{r}) & \Omega_R^{12}\alpha\sin(\mathbf{\Delta}_k\cdot\mathbf{r}) & -\Gamma_{1212} & \Omega_R^{12}\alpha\sin(\mathbf{\Delta}_k\cdot\mathbf{r}) \\ -2\Omega_R^{12}[1+\alpha\cos(\mathbf{\Delta}_k\cdot\mathbf{r})] & -\Omega_R^{12}[1+\alpha\cos(\mathbf{\Delta}_k\cdot\mathbf{r})] & -\omega_{21}+\Omega_p-k_{pz}v_z & -\Omega_R^{12}[1+\alpha\cos(\mathbf{\Delta}_k\cdot\mathbf{r})] \end{vmatrix} \tag{4.10}$$

From the knowledge of the quantities $\rho_{22}^{(0)(0)}(\omega)$, $\rho_{33}^{(0)(0)}(\omega)$, $s_{p(r)}^{(0)(0)}(\omega)$, and $s_{p(i)}^{(0)(0)}(\omega)$ previously established, we calculate the quantity $s_s$ from the third and fifth equalities of Eq. (4.4). This is all that we need to calculate the coherence terms $\rho_{31}(t)$. We get

$$\dot{s}_s^*=[i(\omega_{31}-\Omega_s+k_{sz}v_z)-\Gamma_{1313}]s_s^*+\frac{i}{\hbar}\boldsymbol{\mu}_{12}\cdot\mathbf{E}_p(\Omega_p)r_- + \frac{i}{\hbar}\boldsymbol{\mu}_{13}\cdot\mathbf{E}_s(\Omega_s)(2\rho_{33}^{(0)}+\rho_{22}^{(0)}-1),$$

$$\dot{r}_-=[i(\omega_{32}+\Omega_p-\Omega_s-(k_{pz}-k_{sz})v_z)-\Gamma_{2323}]r_- + \frac{i}{\hbar}\boldsymbol{\mu}_{21}\cdot\mathbf{E}_p^*(\Omega_p)[1+\alpha^* e^{i\mathbf{\Delta}_k\cdot\mathbf{r}}]s_s^*-\frac{i}{\hbar}\boldsymbol{\mu}_{13}\cdot\mathbf{E}_s(\Omega_s)s_p. \tag{4.11}$$

With the partition in real and imaginary parts for $s_s=s_{s(r)}+is_{s(i)}$ and $r_-=r_{-(r)}+ir_{-(i)}$ and introducing a Fourier series expansion for these quantities, we obtain

$$in\omega_{s(r)}^{(n)}(\omega)=-\Gamma_{1313}s_{s(r)}^{(n)}(\omega)+(\omega_{31}-\Omega_s+k_{sz}v_z)s_{s(i)}^{(n)}(\omega) -\Omega_R^{12}r_{-(i)}^{(n)}(\omega),$$

$$in\omega s_{s(i)}^{(n)}(\omega)=-\Gamma_{1313}s_{s(i)}^{(n)}(\omega)-(\omega_{31}-\Omega_s+k_{sz}v_z)s_{s(r)}^{(n)}(\omega) -\Omega_R^{12}r_{-(r)}^{(n)}(\omega)+\Omega_R^{13}(-2\rho_{33}^{(0)}-\rho_{22}^{(0)}+1),$$

$$in\omega r_{-(r)}^{(n)}(\omega)=-\Gamma_{2323}r_{-(r)}^{(n)}(\omega)-[\omega_{32}+\Omega_p-\Omega_s-(k_{pz}-k_{sz})v_z]r_{-(i)}^{(n)}(\omega)+\Omega_R^{(12)} \times[1+\alpha\cos(\mathbf{\Delta}_k\cdot\mathbf{r})]s_{s(i)}^{(n)}(\omega) -\Omega_R^{12}\alpha\sin(\mathbf{\Delta}_k\cdot\mathbf{r})s_{s(r)}^{(n)}(\omega)+\Omega_R^{13}s_{p(i)},$$

$$in\omega r^{(n)}_{-(i)}(\omega)=-\Gamma_{2323}r^{(n)}_{-(i)}(\omega)+[\omega_{32}+\Omega_p-\Omega_s-(k_{pz}-k_{sz})v_z]r^{(n)}_{-(r)}(\omega)+\Omega_R^{12}\times[1+\alpha\cos(\mathbf{\Delta}_k\cdot\mathbf{r})]s^{(n)}_{s(r)}(\omega)+\Omega_R^{12}\alpha\sin(\mathbf{\Delta}_k\cdot\mathbf{r})s^{(n)}_{s(i)}(\omega)-\Omega_R^{13}s_{p(r)}. \tag{4.12}$$

Again, we have the solutions

$$r^{(n)}_{-(i)}(\omega)=r^{(n)}_{-(r)}(\omega)=s^{(0)(n)}_{s(r)}(\omega)=s^{(0)(n)}_{s(i)}(\omega)=0 \quad \text{for } n\neq 0, \tag{4.13}$$

while for $n=0$, with the additional notation

$$\Lambda(n)=\begin{vmatrix} -in\omega-\Gamma_{1313} & \omega_{31}-\Omega_s+k_{sz}v_z & 0 & -\Omega_R^{12} \\ -\omega_{31}+\Omega_s-k_{sz}v_z & -in\omega-\Gamma_{1313} & -\Omega_R^{12} & 0 \\ -\Omega_R^{12}\alpha\sin(\mathbf{\Delta}_k\cdot\mathbf{r}) & \Omega_R^{12}[1+\alpha\cos(\mathbf{\Delta}_k\cdot\mathbf{r})] & -in\omega-\Gamma_{2323} & -\omega_{32}-\Omega_p+\Omega_s+(k_{pz}-k_{sz})v_z \\ \Omega_R^{12}[1+\alpha\cos(\mathbf{\Delta}_k\cdot\mathbf{r})] & \Omega_R^{12}\alpha\sin(\mathbf{\Delta}_k\cdot\mathbf{r}) & \omega_{32}+\Omega_p-\Omega_s-(k_{pz}-k_{sz})v_z & -in\omega-\Gamma_{2323} \end{vmatrix}, \tag{4.14}$$

we have

$$s^{(0)(0)}_{s(r)}(\omega)=\frac{1}{\Lambda(0)}\times\begin{vmatrix} 0 & \omega_{31}-\Omega_s+k_{sz}v_z & 0 & -\Omega_R^{12} \\ \Omega_R^{13}(2\rho^{(0)}_{33}+\rho^{(0)}_{22}-1) & -\Gamma_{1313} & -\Omega_R^{12} & 0 \\ -\Omega_R^{13}s_{p(i)} & \Omega_R^{12}[1+\alpha\cos(\mathbf{\Delta}_k\cdot\mathbf{r})] & -\Gamma_{2323} & -\omega_{32}-\Omega_p+\Omega_s+(k_{pz}-k_{sz})v_z \\ \Omega_R^{13}s_{p(r)} & \Omega_R^{12}\alpha\sin(\mathbf{\Delta}_k\cdot\mathbf{r}) & \omega_{32}+\Omega_p-\Omega_s-(k_{pz}-k_{sz})v_z & -\Gamma_{2323} \end{vmatrix} \tag{4.15}$$

and

$$s^{(0)(0)}_{s(i)}(\omega)=\frac{1}{\Lambda(0)}\times\begin{vmatrix} -\Gamma_{1313} & 0 & 0 & -\Omega_R^{12} \\ -\omega_{31}+\Omega_s-k_{sz}v_z & \Omega_R^{13}(2\rho^{(0)}_{33}+\rho^{(0)}_{22}-1) & -\Omega_R^{12} & 0 \\ -\Omega_R^{12}\alpha\sin(\mathbf{\Delta}_k\cdot\mathbf{r}) & -\mathbf{\Omega}_R^{13}s_{p(i)} & -\Gamma_{2323} & -\omega_{32}-\Omega_p+\Omega_s+(k_{pz}-k_{sz})v_z \\ \Omega_R^{12}[1+\alpha\cos(\mathbf{\Delta}_k\cdot\mathbf{r})] & \Omega_R^{13}s_{p(r)} & \omega_{32}+\Omega_p-\Omega_s-(k_{pz}-k_{sz})v_z & -\Gamma_{2323} \end{vmatrix}. \tag{4.16}$$

If we consider the case where no nonradiative transition occurs, so that $\Gamma_{2233}=\Gamma_{3322}=0$, then with our previous approximation, we have a constant population in level 3, $\rho^{(0)}_{33}=N'$, and Eqs. (4.5) reduce to

$$\begin{aligned} \dot\rho^{(0)}_{22}&=-\Gamma_{2222}\rho^{(0)}_{22}+2\Omega_R^{12}[1+\alpha\cos(\mathbf{\Delta}_k\cdot\mathbf{r})]s^{(0)}_{p(i)}-2\Omega_R^{12}\alpha\sin(\mathbf{\Delta}_k\cdot\mathbf{r})s^{(0)}_{p(r)}, \\ \dot s^{(0)}_{p(r)}&=-\Gamma_{1212}s^{(0)}_{p(r)}+(\omega_{21}-\Omega_p+k_{pz}v_z)s^{(0)}_{p(i)}+\Omega_R^{12}\alpha\sin(\mathbf{\Delta}_k\cdot\mathbf{r})(2\rho^{(0)}_{22}+N'-1), \\ \dot s^{(0)}_{p(i)}&=-\Gamma_{1212}s^{(0)}_{p(i)}-(\omega_{21}-\Omega_p+k_{pz}v_z)s^{(0)}_{p(r)}-\Omega_R^{12}[1+\alpha\cos(\mathbf{\Delta}_k\cdot\mathbf{r})](2\rho^{(0)}_{22}+N'-1). \end{aligned} \tag{4.17}$$

Therefore, the zero-order population of level $|2\rangle$ takes the form

$$\rho^{(0)}_{22}=\frac{2(\Omega_R^{12})^2\Gamma_{1212}(1-N')[1+\alpha^2+2\alpha\cos(\mathbf{\Delta}_k\cdot\mathbf{r})]}{\Gamma_{2222}[\Gamma^2_{1212}+(\omega_{21}-\Omega_p+k_{pz}v_z)^2]+4(\Omega_R^{12})^2\Gamma_{1212}[1+\alpha^2+2\alpha\cos(\mathbf{\Delta}_k\cdot\mathbf{r})]}. \tag{4.18}$$

Similarly, with the same approximation on the probe beam we obtain, for the real and imaginary parts of the factor $s_p = s_{p(r)} + i s_{p(i)}$, the expressions

$$s_{p(r)}^{(0)} = \frac{\Gamma_{2222}\Omega_R^{12}(N'-1)\{\Gamma_{1212}\alpha \sin(\boldsymbol{\Delta}_k \cdot \mathbf{r}) - (\omega_{21} - \Omega_p + k_{pz}v_z)[1 + \alpha \cos(\boldsymbol{\Delta}_k \cdot \mathbf{r})]\}}{\Gamma_{2222}[\Gamma_{1212}^2 + (\omega_{21} - \Omega_p + k_{pz}v_z)^2] + 4(\Omega_R^{12})^2\Gamma_{1212}[1 + \alpha^2 + 2\alpha \cos(\boldsymbol{\Delta}_k \cdot \mathbf{r})]},$$

$$s_{p(i)}^{(0)} = \frac{\Gamma_{2222}\Omega_R^{12}(1-N')\{\Gamma_{1212}[1 + \alpha \cos(\boldsymbol{\Delta}_k \cdot \mathbf{r})] + (\omega_{21} - \Omega_p + k_{pz}v_z)\alpha \sin(\boldsymbol{\Delta}_k \cdot \mathbf{r})\}}{\Gamma_{2222}[\Gamma_{1212}^2 + (\omega_{21} - \Omega_p + k_{pz}v_z)^2] + 4(\Omega_R^{12})^2\Gamma_{1212}[1 + \alpha^2 + 2\alpha \cos(\boldsymbol{\Delta}_k \cdot \mathbf{r})]}. \tag{4.19}$$

From the knowledge of $\rho_{22}^{(0)}$ and $s_p^{(0)}$ previously established, the coefficient $s_s$ is straightforwardly obtained. This is all that we need to calculate the coherence terms $\rho_{31}(t)$ required for the evaluation of the TC-RFWM spectrum. Its expression will enable us to discuss the influence of the dynamical constants on the spectra and to elucidate the origin of the asymmetry recently observed in the TC-RFWM spectra in jet-cooled CH [34]. Also, we will fit the experimental data to determine the corresponding total decay rates and dephasing constants. The evaluation of the signal intensity lies on the evaluation of the polarization $\mathbf{P}_{\mathbf{k}_s}(\Omega_s)$ along the direction of the probe beam $\mathbf{k}_s$ for the transition $|1\rangle \rightarrow |3\rangle$. Therefore, the corresponding intensity can be straightforwardly deduced from the expression

$$I(\Omega_p) = |\mathbf{P}_{\mathbf{k}_s}(\Omega_s)|^2 = |\rho_{31}(\mathbf{k}_s, \Omega_s)\boldsymbol{\mu}_{13}|^2 = |s_{s(r)}^{(0)} + i s_{s(i)}^{(0)}|^2, \tag{4.20}$$

where $\rho_{31}(\mathbf{k}_s, \Omega_s)$ corresponds, to first order on the probe beam, to the Fourier component of the density matrix in the $\mathbf{k}_s$ direction for the transition $|1\rangle \rightarrow |3\rangle$. Notice that both quantities $s_{s(r)}^{(0)}$ and $s_{s(i)}^{(0)}$ depend on $\rho_{22}^{(0)}$, $s_{p(r)}^{(0)}$, and $s_{p(i)}^{(0)}$ previously evaluated and given by Eqs. (4.10) in the general case. Their expressions reduce to Eqs. (4.18) and (4.19) when the nonradiative constants cancel. These quantities are exactly what is required to fit the experimental data on the TC-RFWM signal intensity. Of course, other geometries can be treated along the same lines.

Like in the preceding section, we come now to some numerical simulations to illustrate the peculiar features observed in this spectroscopic configuration. First of all, we want to emphasize the influence of the pure dephasing processes described by $\Gamma_{12}^{(d)}$ and $\Gamma_{13}^{(d)}$ and acting on the transitions 1-2 and 1-3, respectively. The variations are shown in Fig. 6. We begin with the pure dephasing processes acting on the transition 1-2 driven by the strong grating fields. Here, because we are in the strong-field regime, the pure dephasing constant $\Gamma_{12}^{(d)}$ contributes to the generalized Rabi frequency by increasing it, and consequently increases the line splitting. This is why we note an increase of the dip with the increase of $\Gamma_{12}^{(d)}$. However, concerning the influence of the pure dephasing processes accounted for by $\Gamma_{13}^{(d)}$ and acting on the 1-3 transition driven by the weak probe field, the increase of the pure dephasing constant tends to wash out the dip structure. It can be mentioned that in supersonic molecular jet beams, the microscopic processes accounted for by the dephasing constants correspond mainly to elastic collisions

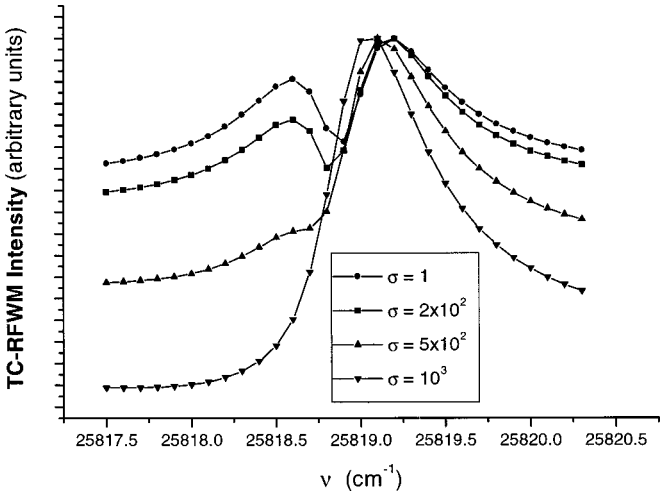


FIG. 8. Influence of the transverse velocity distribution on the TC-RFWM spectra for different values of the distribution width $\sigma$ given in the inset. The frequency of the probe beam is resonant with the 1-3 transition frequency. Other values are similar to those of Fig. 7.

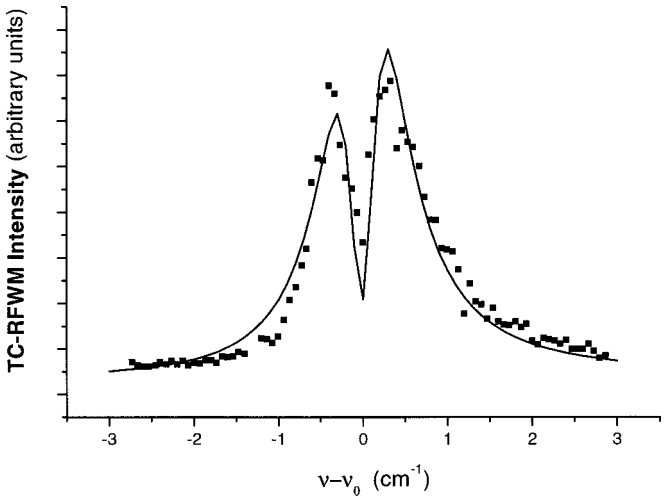


FIG. 9. Fit on the TC-RFWM spectrum of the $R_1(2)$ line of the *B-X* (0-0) vibronic band obtained for a *YYYY* polarization scheme and a total energy of the grating beam of 100 $\mu$J in the ground-state grating configuration. The experimental points correspond to the squares and the solid line represents our predictions from the model.

occuring between the molecules in the jet. We note that the residual TC-RFWM signal is always present in this experiment, since we are tuning the grating beams at fixed probe field frequency and detecting the signal resulting from the polarization of the 1-3 transition. The TC-RFWM signal depends on $\Gamma_{13}^{(d)}$ far from resonance. In addition, we can mention that the asymmetry of the spectra result from a nonzero molecular transverse velocity as will be discussed in the following. Next, we analyze the influence of the transverse molecular velocity of the jet-cooled beam on the TC-RFWM spectrum. The Doppler shift, resulting from the transverse molecular motion, alters the diffraction of the probe beam by the grating created by the two fields $\mathbf{E}_p$. According to the sign of the velocity component, this modification results in constructive or destructive interferences, depending on whether the frequency of the grating beams is higher or lower than the transition frequency. To emphasize this point, the spectra have been drawn for different values of the transverse velocity component. First of all, we note that the spectra obtained for opposite values of this velocity component are symmetric with respect to the frequency of the 1-2 transition. Of course, for zero value of the velocity, the spectrum recovers a complete symmetry independently of the relaxation and dephasing constants. As the grating beams are intense enough to split the spectral line, all the constants are symmetrized. This clearly shows that no asymmetry can be expected from the internal structure of the three-level model, as previously mentioned. The corresponding variations of the spectra are shown in Fig. 7. They show that positive values of the velocity component give constructive interferences for $\Omega_p < \omega_{21}$ and vice versa. It is interesting to note that the influence of the transverse velocity on the TC-RFWM spectrum appears yet at small values of the component. Besides, due to the experimental setup, the molecules can have a transverse velocity distribution in the jet. Then, a Gaussian function can be used to model the transverse velocity distribution and to evaluate the average TC-RFWM spectrum. As we can see from Fig. 8, the main consequence of this distribution is to wash out the double resonance structure and simultaneously to partially reduce the spectral asymmetry.

Finally, we take advantage of our description to fit the experimental data obtained on a jet-cooled CH produced by the photolysis of $CHBr_3$, using GSG spectroscopy [34]. In this experiment, the *YYYY* polarization scheme has been chosen because it shows the least threshold energy for saturation. In this experiment two nearly parallel grating beams, which cross at a small angle of about 1°, propagate nearly perpendicularly to the jet-cooled CH. The probe beam propagates in the opposite direction and crosses the grating beams at a small angle to match the phase. The experimental geometry is shown in Fig. 1. The TC-RFWM spectrum investigated in this experiment corresponds to the $R_1(2)$ line of the $B$-$X$ (0-0) vibronic band. To this end, the common frequency of both grating beams is tuned around the $B$-$X$ (0-0) transition corresponding to 25 818.90 $cm^{-1}$, while the fixed probe beam frequency is resonant with the $A$-$X$ (0-0) transition frequency of 23 460.96 $cm^{-1}$. The spectroscopic properties of the CH radical have been widely studied [38–43]. The low-lying configurations $X\ ^2\Pi$, $B\ ^2\Sigma^-$, and $A\ ^2\Delta$ of CH are well characterized and correspond to the model states $|1\rangle$, $|2\rangle$, and $|3\rangle$, respectively. The more important features appearing in the TC-RFWM spectra are certainly the line splittings obtained for increasing values of the grating beam intensities, and the asymmetry, which is again more likely observed for intense grating beams. Notice that this asymmetry still remains even at low grating beam intensities, but of course, with a much smaller magnitude. While the line splitting has been interpreted on the basis of a theory developed for DFWM by Meacher and co-workers [30–32], a theory initially based on the Abrams-Lind model [27–29], or even by using the concept of anharmonic gratings [44,45], they failed to explain the spectral asymmetry. Notice that all these previous theories predict the same double-resonance spectral structure symmetric with respect to the central dip. Of course, their results are recovered by the present model when the transverse molecular velocity goes to zero. In our model, its evaluation results strictly from the dynamical evolution of the moving molecules with nonzero transverse velocity and described by a three-level model excited by the grating fields applied on the $|1\rangle \rightarrow |2\rangle$ transition, while the probe field acts on the $|1\rangle \rightarrow |3\rangle$ transition. While the present model can be applied to any experimental geometry, the experimental data on jet-cooled CH have been obtained with identical grating beams except for the direction of their wave vectors, as indicated previously. In Fig. 9, we fit the experimental data obtained for a total grating beam intensity of 100 $\mu$J. The fit of the experimental data obtained for a total grating beam intensity of 10 and 50 $\mu$J gave the value $\Gamma_{2222} = 0.35\ cm^{-1}$. Not much is known about total decay rates or dephasing constants for these transitions, making any speculation on this value quite difficult. Notice that $\Gamma_{2222}$ is characteristic from the CH rotational structure and has nothing to do with the photolysis process producing the CH molecule. Also, we have to mention that the fit is less sensitive to the value of $\Gamma_{3333}$. For this reason, it has been chosen equal to $\Gamma_{2222}$. Finally, due to the strong influence of the transverse velocity on the spectra, the influence of the pure dephasing processes are masked and their corresponding constants have been set to zero. Of course, for smaller values of the transverse velocity or more precise experimental data, which implies controlling the distribution of $v_z$, the determination of the dephasing constants could be realized. Finally, from the fit shown in Fig. 9, we obtain a velocity component of $v_z = -42$ m/s, a value that seems quite reasonable for this type of experiment. The fact that only the negative value of $v_z$ is found in the experiment indicates that the laser beam was mainly focused on the jet zone, where the expansion gives a transverse molecular velocity in the opposite sense to the grating beam propagation. Notice that a situation involving both positive and negative values of $v_z$ will have contributions that will restore the symmetry of the spectral line.

## V. CONCLUSION

In this work, we have presented a general description of TC-RFWM valid for V- and Λ-type models. These models previously applied in atomic physics have been generalized to account for nonradiative transitions between the molecular

excited states as well as rotational or vibrational dephasings. Here, the dephasings are not necessarily the same for both transitions, a simplification previously introduced in the internal dynamics induced by a bichromatic fields acting on the V model, to get an analytical solution [9]. For convenience, because experimental data exist for molecular V models, this model has been treated explicitly. However, the extension to Λ-type models is straightforward with small changes. In addition, our description is valid for any intensity regime of the grating fields. The present analysis shows a high sensibility of the TC-RFWM spectrum to parameters such as transition constants and pure dephasing constants. However, as the grating beams are intense enough to split the spectral line, these constants, which drive the internal dynamics, are redistributed and the TC-RFWM spectrum remains symmetric. This is not the case for the transverse velocity, which exhibits a great influence on the diffraction grating created by the pumping beams and responsible for the strong asymmetry of the TC-RFWM spectrum. Yet notice that this transverse Doppler effect is efficient at small velocities.


[1] Y. R. Shen, *The Principle of Nonlinear Optics* (Wiley-Interscience, New York, 1984).
[2] S. Mukamel, *Principles of Nonlinear Optical Spectroscopy* (Oxford University Press, New York, 1995).
[3] P. Ewart and S. V. O'Leary, Opt. Lett. **11**, 279 (1986).
[4] R. L. Farrow and D. J. Rakestraw, Science **257**, 1894 (1992).
[5] S. Williams, R. N. Zare, and L. A. Rahn, J. Chem. Phys. **101**, 1093 (1994).
[6] T. Dreier and D. J. Rakestraw, Opt. Lett. **15**, 72 (1990).
[7] T. J. Buthenoff and E. A. Rohlfing, J. Chem. Phys. **97**, 1595 (1992).
[8] A. Valli and S. Stenholm, Phys. Lett. **64A**, 447 (1978).
[9] M. Z. Smirnov, J. Opt. Soc. Am. B **9**, 2171 (1992).
[10] O. Emile, R. Kaiser, C. Gertz, H. Wallis, A. Aspect, and C. Cohen-Tannoudji, J. Phys. II **3**, 1709 (1993).
[11] T. Cai and N. P. Bigelow, Opt. Commun. **104**, 175 (1993).
[12] H. Wallis, Phys. Rev. A **52**, 1441 (1995).
[13] S. F. Yelin, M. D. Lukin, M. O. Scully, and P. Mandel, Phys. Rev. A **57**, 3858 (1998).
[14] J. Kitching and L. Hollberg, Phys. Rev. A **59**, 4685 (1999).
[15] E. F. McCormack, S. T. Pratt, P. M. Dehmer, and J. L. Dehmer, Chem. Phys. Lett. **211**, 143 (1993).
[16] E. F. McCormach, S. T. Pratt, P. M. Dehmer, and J. L. Dehmer, Chem. Phys. Lett. **227**, 656 (1994).
[17] M. A. Buntine, D. W. Chandler, and C. C. Hayden, J. Chem. Phys. **97**, 707 (1992).
[18] S. Williams, J. D. Tobiason, J. R. Dunlop, and E. A. Rohlfing, J. Chem. Phys. **102**, 8342 (1995).
[19] S. Williams, R. N. Zare, and L. A. Rahn, J. Chem. Phys. **101**, 1072 (1994).
[20] J. Ishii, K. Uehara, and K. Tsukiyama, J. Chem. Phys. **102**, 9174 (1995).
[21] E. F. McCormack, F. D. Teodoro, and J. M. Grochocinski, J. Chem. Phys. **109**, 63 (1998).
[22] A. Kumar, W. C. Hung, C. C. Hsiao, and Y. P. Lee, J. Chem. Phys. **109**, 3824 (1998).
[23] X. Li, A. Kumar, C. C. Hsiao, and Y. P. Lee, J. Phys. Chem. A **103**, 6162 (1999).
[24] F. D. Teodoro and E. F. McCormack, Phys. Rev. A **57**, 162 (1998).
[25] S. Williams, E. A. Rohlfing, L. Rahn, and R. N. Zare, J. Chem. Phys. **106**, 3090 (1997).
[26] E. F. McCormack and E. Sarajlic, Phys. Rev. A **63**, 023406 (2001).
[27] R. L. Abrams and R. C. Lind, Opt. Lett. **2**, 94 (1978).
[28] R. L. Abrams and R. C. Lind, Opt. Lett. **3**, 205 (1978).
[29] R. L. Abrams, J. F. Lam, R. C. Lind, D. G. Steel, and P. F. Liao, in *Optical Phase Conjugation*, edited by R. A. Fisher (Academic, New York, 1983).
[30] D. R. Meacher, A. Charlton, P. Ewart, J. Cooper, and G. Alber, Phys. Rev. A **42**, 3018 (1990).
[31] G. Alber, J. Cooper, and P. Ewart, Phys. Rev. A **31**, 2344 (1985).
[32] J. Cooper, A. Charlton, D. R. Meacher, P. Ewart, and G. Alber, Phys. Rev. A **40**, 5705 (1989).
[33] J. R. Dunlop and E. A. Rohlfing, J. Chem. Phys. **100**, 856 (1994).
[34] A. Kumar, C. C. Hsiao, Y. Y. Lee, and Y. P. Lee, Chem. Phys. Lett. **297**, 300 (1998).
[35] A. Bambini, Phys. Lett. **58A**, 3 (1976).
[36] C. Cohen-Tannoudji, J. Dupont-Roc, and G. Grynberg, *Processus d'Interaction entre Photons et Atomes, Savoirs Actuels* (InterEditions/Editions du CNRS, Paris, 1988).
[37] V. G. Minogin and T. Serimaa, Opt. Commun. **30**, 373 (1979).
[38] P. F. Bernath, C. R. Brazier, T. Olsen, R. Hailey, W. T. M. L. Fernando, C. Woods, and J. L. Hardwick, J. Mol. Spectrosc. **147**, 16 (1991).
[39] P. F. Bernath, C. R. Brazier, T. Olsen, R. Hailey, W. T. M. L. Fernando, C. Woods, and J. L. Hardwick, J. Mol. Spectrosc. **149**, 563 (1991).
[40] P. F. Bernath, C. R. Brazier, T. Olsen, R. Hailey, W. T. M. L. Fernando, C. Woods, and J. L. Hardwick, J. Mol. Spectrosc. **165**, 301 (1994).
[41] P. F. Bernath, J. Chem. Phys. **86**, 4838 (1987).
[42] J. Luque and D. R. Crosley, J. Chem. Phys. **104**, 2146 (1996).
[43] J. Luque and D. R. Crosley, J. Chem. Phys. **104**, 3907 (1996).
[44] D. J. McGraw, J. Michaelson, and J. M. Harris, J. Chem. Phys. **86**, 2536 (1987).
[45] X. R. Zhu and J. M. Harris, J. Phys. Chem. **93**, 75 (1989).